



BALLISTIC IMPACT CRATER MODELLING USING UAV
AND STRUCTURE FROM MOTION TECHNOLOGY

2012 Te Maari Volcanic Eruptions, New Zealand



A thesis submitted in partial fulfilment of the
requirements for the Degree of
Masters in Geographic Information Systems
(MGIS)

At

The University of Canterbury

By

Ravitej Pitchika

2017

Abstract

New Zealand has a strong historical background of producing volcanic eruptions and earthquakes due to its geographical setting. The deformation caused by the collision of Australian and Pacific plates has given rise to New Zealand's volcanism. Most of NZ's volcanism has occurred in the Taupo Volcanic Zone (TVZ) in the last 1.6 million years. On 6th August 2012, Upper Te Maari volcanic eruptions occurred on the north-eastern flanks of Tongariro volcano complex, in TVZ region producing a hazard from volcanic ballistic projectiles. The vulnerability of people walking along the Tongariro Alpine Crossing to ballistic impacts was identified by (Fitzgerald, 2014) and the hazard was calculated by remote and field mapping of ballistic craters.

This project examines the effectiveness and accuracy of mapping a volcanic crater field near Tongariro, using a Draganfly X4P un-manned aerial vehicle (UAV). The UAV is flown at different elevations above the ground surface to capture the two-dimensional ground images. The UAV imagery datasets and ground truthing survey points are incorporated to Agisoft Photoscan Pro software to build a three-dimensional elevation model, using Structure from motion (SfM) and photogrammetry technology. The use of UAV's and SfM to study geohazards is a new concept which could prove an alternative to the more expensive Light Detection and Ranging (LiDAR) surveys.

The digital elevation models (DEMs) developed in SfM photogrammetric software were used to identify volcanic craters within a 100 m² survey site selected for this project. A model was built using six different parameters, to distinguish volcanic craters from natural depressions on the ground surface. The UAV's imagery resolution, altitude of the flight and other atmospheric factors play a crucial role to

the accuracy of the results. A total of 135 volcanic craters were identified with 118 pixels per centimetre (ppcm), when the UAV was flown at 40m altitude above the ground surface. When the resolution of images was reduced to 70 ppcm manually, only 101 volcanic craters could be identified successfully.

A LiDAR is a remote sensing method used to measure variable distances to the Earth that uses near infrared pulsed laser to map the topographic land surface. A LiDAR and aerial imagery survey was first conducted by NZ Aerial Mapping in November 2012, three months after the 2012 Te Maari volcanic eruptions. Out of the total 3587 volcanic craters yielded from LiDAR and orthophoto analysis, 107 craters fall within the 100 m² survey site chosen in for this project (Fitzgerald, 2014). The UAV and SfM modelling identified more craters (135) four years post 2012 Te Maari eruptions. This thesis found that UAV's are both feasible and cost-effective when used in this context; however, the major limiting factor is the small area covered by a UAV when compared to LiDAR surveys. Hence, the SfM and UAV technology can therefore be used at localized sites to achieve maximized results with cost effective measures, when compared to conducting LiDAR surveys.

Acknowledgements

I would like to thank my supervisors Ben Kennedy and Christopher Gomez from University of Canterbury for providing me the right guidance during the thesis year. They were amazing to deal with and I consider myself very lucky to have them as my supervisors. Huge thanks to both Geology and Geography department faculty members who I have dealt with, for accommodating and providing me the resources required to undergo this study.

I would also like to thank Rod Hope from Land Information New Zealand for showing me how laser scanning works and Nick Key, Paul Bealing from UAV department at University.

My parents have been a great inspiration to me so, I thank them for supporting me throughout my time at UC.

Contents

Abstract	i
Acknowledgements	iii
List of Figures	vi
List of Tables.....	vii
Chapter 1: Introduction	1
1.1 Context of study	1
1.2 Research Questions	2
1.3 Structure of Thesis.....	2
Chapter 2: Literature Review	4
2.1 Introduction.....	4
2.2 Understanding the eruption style.....	4
2.3 Te Maari eruptions 2012	6
2.4 Applications of photogrammetry and structure from motion (SfM)	7
2.5 GNSS Equipment for ground-truthing	8
2.6 UAV and camera setup specifications.....	10
2.6.1 Draganfly X4P UAV	10
2.6.2 Sony RX100	11
2.7 Computer Processing Requirements.....	12
Chapter 3: Research Component.....	13
3.1 Fieldwork Methodology	13
3.1.1 Study Area	13
3.1.2 Draganfly UAV Flight and GCPs	15
3.1.3 Ground Truthing using Trimble GNSS R8 and TSC3 Controller.....	19
3.2 Agisoft Photoscan Pro workflow.....	21

Chapter 4: Results.....	30
4.1 Role of Geographic Information Systems (GIS) and SfM for volcanic crater modelling	30
4.2 Identifying craters using SfM.....	32
4.3 GNSS versus DEM generated measurements	34
4.4 Image Resolution and its effect on DEM.....	37
Chapter 5: Discussion.....	39
5.1 Explanation of Error Map	39
5.2 Conclusions from Data	42
5.2.1 Technical aspects, limitations and costs involved	47
5.3 Considerations for future SfM field methods	49
5.4 Hazard Risks and Management of UAV hazards.....	50
Chapter 6: Conclusion.....	52
References.....	54

List of Figures

Figure 1: Trimble R8 GNSS system and TSC3 controller (Source: AGS, 2016)	8
Figure 2: Base and rover connectivity for PPK style of survey	9
Figure 3: Draganfly X4P UAV and Sony RX100 camera setup (Source: Draganfly, 2017)	10
Figure 4: Selected study site within the August 2012 volcanic ballistic crater field	14
Figure 5: Volcanic hazard zone radius of future Te Maari eruption (Source: Department of conservation, NZ)	14
Figure 6: GCP target design for identification purpose on ground surface	16
Figure 7: GCP targets from 20m elevation (top) and 40m elevation (bottom) taken from Draganfly X4P UAV	18
Figure 8: Range and variations of volcanic craters at Te Maari eruption site (images taken in 2016)	20
Figure 9: Photoscan Pro SfM workflow to create digital elevation model	21
Figure 10: Flight 1 imagery dataset (91 images) a) post image-alignment (top left) b) dense point cloud (top right) c) post build-mesh (bottom left) d) post build texture (bottom right)	22
Figure 11: Flight 2 imagery dataset (145 images) a) post image-alignment (top left) b) dense point cloud (top right) c) post build-mesh (bottom left) d) post build texture (bottom right)	23
Figure 12: DEM of imagery 1 dataset in SfM Photoscan Pro software	24
Figure 13: Camera locations and image overlap of flight 1 dataset	25
Figure 14: SfM resolution survey details of flight 1 dataset	25
Figure 15: Image residuals for DSC-RX100M3 (8.8 mm) camera calibration of flight 1 dataset	26
Figure 16: Camera locations and image overlap of flight 2 dataset	27
Figure 17: SfM resolution survey details of flight 2 dataset	27
Figure 18: Image residuals for DSC-RX100M3 (8.8mm) camera calibration of flight 2 dataset	28
Figure 19: Ground control point locations of flight 1 dataset	29
Figure 20: a) Density pattern of GCPs (top) b) Optimised hotspot analysis of GCPs	31
Figure 21: SfM generated DEM elevation profile versus GNSS measured elevation profile at Te Maari	35
Figure 22: Expected values of elevation profile against measured GNSS elevation profile	36
Figure 23: Orthophoto of low resolution dataset 70ppcm	38
Figure 24: Elevation map of Imagery 1 Draganfly X4P Dataset	40
Figure 25: GNSS versus DEM elevation profile error map at Te Maari	41
Figure 26: Locations of 135 volcanic craters identified using a model builder	43

List of Tables

<i>Table 1: Agisoft Photoscan Pro configuration requirements (Source: Agisoft, 2017)</i>	12
<i>Table 2: Some examples of ground truthing data collection of GCPs and natural features</i>	17
<i>Table 3: GCP locational error values of flight 1 dataset</i>	29
<i>Table 4: Point score model to identify volcanic craters</i>	33
<i>Table 5: Comparison of different techniques and survey styles</i>	44
<i>Table 6: Hazard risk assessment and management when conducting UAV SfM flight</i>	50

Chapter 1: Introduction

1.1 Context of study

A disaster is a sudden, calamitous event that disrupts the functioning of a society and causes human, infrastructure and economic loss that exceed the community's ability to cope using its own resources (Turner, Lucieer, & Watson, 2012). Any event that poses a level of threat to life, property or environment is considered a hazard. NZ consists of many volcanoes and its eruption type can vary minute to minute.

Volcanic ballistic projectiles such as rockfall, blocks, bombs that eject from explosive volcanic eruptions produce many proximal hazards to humans, buildings, infrastructure and environment. This study is to find a quick cost efficient method to map the hazards from volcanic eruptions, to minimize the volcanic hazard threat. The common methods used to map large areas include remote sensing, satellite imagery and LiDAR survey methods. However, these are cost prohibitive and time consuming methods to process data.

Resolution and accuracy of aerial imagery plays an important role in mapping natural hazards. This research is vital to establish the most time and resource-economic method for mapping ballistic impact craters, to improve hazard assessments at volcanoes.

UAV's have started to appear in many fields especially environmental management, remote sensing and even in the monitoring of animal and marine life (Prakash et al., 2014). A combination of UAV and SfM photogrammetry technology are used in this research to understand its potential in volcanic hazard mapping.

1.2 Research Questions

This study aims to highlight the importance of UAV assessments in volcanic hazard management scenarios. This will be achieved through:

- Producing digital elevation models (DEMs) in photogrammetry software by flying an unmanned aerial vehicle (UAV) at various height intervals. The DEMs are essential to compare the results against previously conducted small scale UAV assessments and LiDAR based assessments (Fitzgerald, 2014).
- Distinguishing the volcanic ballistic craters from the Te Maari 2012 eruption on the ground surface from other natural depressions by developing geological parameters and survey criteria for a crater identification model.
- Discussion of image resolutions of the datasets used to create DEMs in Agisoft photoscan pro photogrammetry software.
- A comparison between elevation measurements between GNSS R8 equipment and SfM generated DEM's at different resolutions to produce recommendations for future studies.

1.3 Structure of Thesis

- Chapter 1 provides an overview of ballistic hazards and its effects from a volcanic eruption. It aims to highlight the importance of UAV and SfM in volcanic hazard management scenarios.
- Chapter 2 is focussed on volcanic eruption style through a literature review on the 2012 Te Maari eruption sequence, ballistic impacts, craters, applications and limitations of SfM photogrammetry, UAV and survey equipment set up.

- Chapter 3 is the research component of thesis outlining the methods used for data collection, field methodology, UAV flight, ground truthing using GNSS and SfM workflow.
- Chapter 4 provides further insight into the study of crater identification through SfM workflow processes and how resolution of images play a critical role for future recommendations.
- Chapter 5 is a comparison between elevation measurements between GNSS and SfM generated DEM profile, explaining the elevation error maps. It also provides information for the user to make own decisions comparing different survey methods and equipment needed for future imagery projects.

Chapter 2: Literature Review

2.1 Introduction

A literature review was conducted to address the thesis research objectives by understanding the volcano behaviour at the study site. The pre-event activity prior to the 6th August 2012 Te Maari volcanic eruption, allowed to understand the eruptive style and identify the volcanic hazards, impacting human life and infrastructure. Although volcanic eruptions produce a variety of hazards, this research focusses entirely on mapping ballistic hazards using UAVs and SfM technology. UAV's have experienced an exponential growth in recent years and are being used in very diverse roles, such as geomorphological and erosion studies. Published SfM models have been reviewed to understand the field methods and applying it to volcanic ballistic hazards. With the development of photogrammetric software such as SfM and various open source UAV systems, this technology is adopted in the field of volcanology to accurately map ballistic craters and compare its results with LiDAR surveys.

2.2 Understanding the eruption style

The volcanic eruption style depends on many factors such as magma temperature, chemistry, viscosity, ground water, gas content and deep earth mechanism. The major types of eruptions are as follows:

- Hydrothermal eruption: These are shallow small eruptions and do not include any magma. Ideally driven by heat caused by the steam underground in the hydrothermal system; steam and ash may be observed. These eruptions are short lived and generally one-off events.

- Phreatic eruption: These eruptions occurs when magmatic heat interacts with surface or ground water. The instant evaporation of water to steam results in explosion of steam, ash, rock and blocks.
- Phreatomagmatic eruption: When new magma interacts with ground or surface water, these explosive eruptions occur. Steam, ash, rock, blocks and bombs (ballistic projectiles) are often observed.

Other eruptions such as Strombolian, Hawaiian, Vulcanian, Sub-plinian and Plinian eruptions are measured by the eruption column sizes; often cause major economic damage to the society. These eruptions are also an important natural cause of climate change across many timescales producing greenhouse gases, aerosols and ozone depleting chemicals into the atmosphere (Robock, 2000).

Ballistic projectiles are usually blocks and bombs, which travel like cannonballs from an erupting volcano. These projectiles travel at high energies, capable of destroying infrastructure causing injuries and death to both livestock and people. The Tongariro Alpine Crossing is a 19.4 km track through the volcanic peaks of Ruapehu, Ngauruhoe and Tongariro in NZ. It ranks among the top ten single day treks in the world visited by many tourists each year, even though they are prone to many volcanic geohazards.

2.3 Te Maari eruptions 2012

Mt. Tongariro is a 1978 m high multi vent andesitic volcano located in New Zealand and its eruption products include hydrothermal and subduction composition material. It was formed by volcanic eruptions over the past 275,000 years from at least 12 different vents.

Te Maari craters are named after a Maori chief, Te Maari who died in 1868 after a volcanic eruption (Hobden, 1997). These craters are located on the north-eastern flanks of Tongariro. A series of complex hydrothermal volcanic eruptions occurred on 6th August 2012 at Upper Te Maari in New Zealand. Although considered small by global standards, the eruptive sequence released $\sim 3 \times 10^{12}$ joules (Jolly et al., 2014). Eye witnesses reveal three explosions occurred in quick succession within less than 20 seconds, causing eastward and westward directed blasts producing pyroclastic density currents (PDCs). A final vertical blast produced an ash plume column ~ 7.8 km above mean sea level (Crouch, Pardo, & Miller, 2014). Observations from the seismo-acoustic network were considered to determine the timing of these directional blasts as they were no eye witnesses due to poor night time visibility issues (Lube et al., 2014).

The GeoNet monitoring network first recognised the unrest on 13th July 2012 when a series of volcano-tectonic and high frequency earthquakes were recorded. A total of 120 earthquakes with a magnitude range of 0.8 – 2.9 M_L were recorded prior to the volcanic eruption sequence on 6th August 2012 (Pardo et al., 2014). Increased seismic and hydrothermal activity since July 2012 started the volcanic eruption sequence producing pyroclastic density currents, overlapping ballistic deposits, near surface mass movements, large scarp failure and a debris avalanche (volume of $\sim 7 \times 10^5$ m³) (Procter et al., 2014). Spatial distribution, lithology, ballistic trajectory

models, impact densities and crater analysis allowed eruption sequence interpretation and dynamics (Breard et al., 2014).

2.4 Applications of photogrammetry and structure from motion (SfM)

Due to the technological changes and widespread adoption of digital imagery in the 21st century, applications of photogrammetry can be seen both in theory and practice (McGlone, Mikhail, & Bethel, 1980). Photogrammetry is the art, science and technology of obtaining information of the real world or physical objects by capturing photos and recreating a digital representation of it. It is a process where the photos can either be taken aerially or close-range, and processed in a photogrammetry software for digital elevation model (DEM) generation. Aerial photography involves a real-world object being captured by an aircraft or unmanned aerial vehicle (UAV), by mounting a camera so that it points towards the object. The output of aerial photogrammetry aids in soil and land surveys (Martin, 1980; Peter Heng, Chandler, & Armstrong, 2010), urban and rural development (McGuire, Rys, and Rys 2016), erosion investigations (Mancini et al., 2013), coastal surveys (Maguire, 2014) and topographic products; such as terrain models (Niethammer, Rothmund, James, Travelletti, & Joswig, 2010), topographic maps (Lucieer, Robinson, Turner, Harwin, & Kelcey, 2012), 3-dimensional models and point clouds (Eisenbeiss & Zhang, 2006; Turner et al., 2012). Close range photography usually consists of hand-held imagery (James & Quinton, 2014; Pollefeys et al., 2004) or tripod-monopod imagery (Miller, Morgenroth, & Gomez, 2015) so that the camera is close to the subject. Usually close-range photography is used for non-topographic product purposes; however, it

can be applied to topographic studies especially in places where UAV's cannot be flown.

Structure from motion (SfM) is a cost effective and revolutionary user friendly photogrammetric technique for obtaining high resolution datasets at a range of scales. SfM is an inexpensive, effective and flexible approach to capturing complex topography; and a major advancement in the field of photogrammetry for geoscience applications (Westoby, Brasington, Glasser, Hambrey, & Reynolds, 2012). SfM only requires limited ground control points on the ground surface and it is ideally suited if there are time constraints. Hand held image acquisitions from an aerial platform for the generation of terrain models have begun to emerge recently, with the growing spectrum of photogrammetric software now available (Javernick, Brasington, & Caruso, 2014). However, it is important to note that failure to use ground control points results in lower accuracies (6 to 10 times) than projects that utilize ground control points (Maguire, 2014; Turner et al., 2012).

2.5 GNSS Equipment for ground-truthing



Trimble's R8 GNSS system and TSC3 controller were used to ground truth the ballistic crater field caused by the 2012 Te Maari eruptions. The R8 GNSS system is a rugged and compact unit providing ultimate flexibility for rover and base mode

Figure 1: Trimble R8 GNSS system and TSC3 controller (Source: AGS, 2016)

operations as shown in Figure 1. Four rechargeable and removable 7.4 V, 2.6 Ah Lithium-Ion batteries were used in the field to ground truth a 100 m² area by foot. The unit must be in rover mode to execute a post processed kinematic (ppk) survey and it is set up as shown in Figure 2.

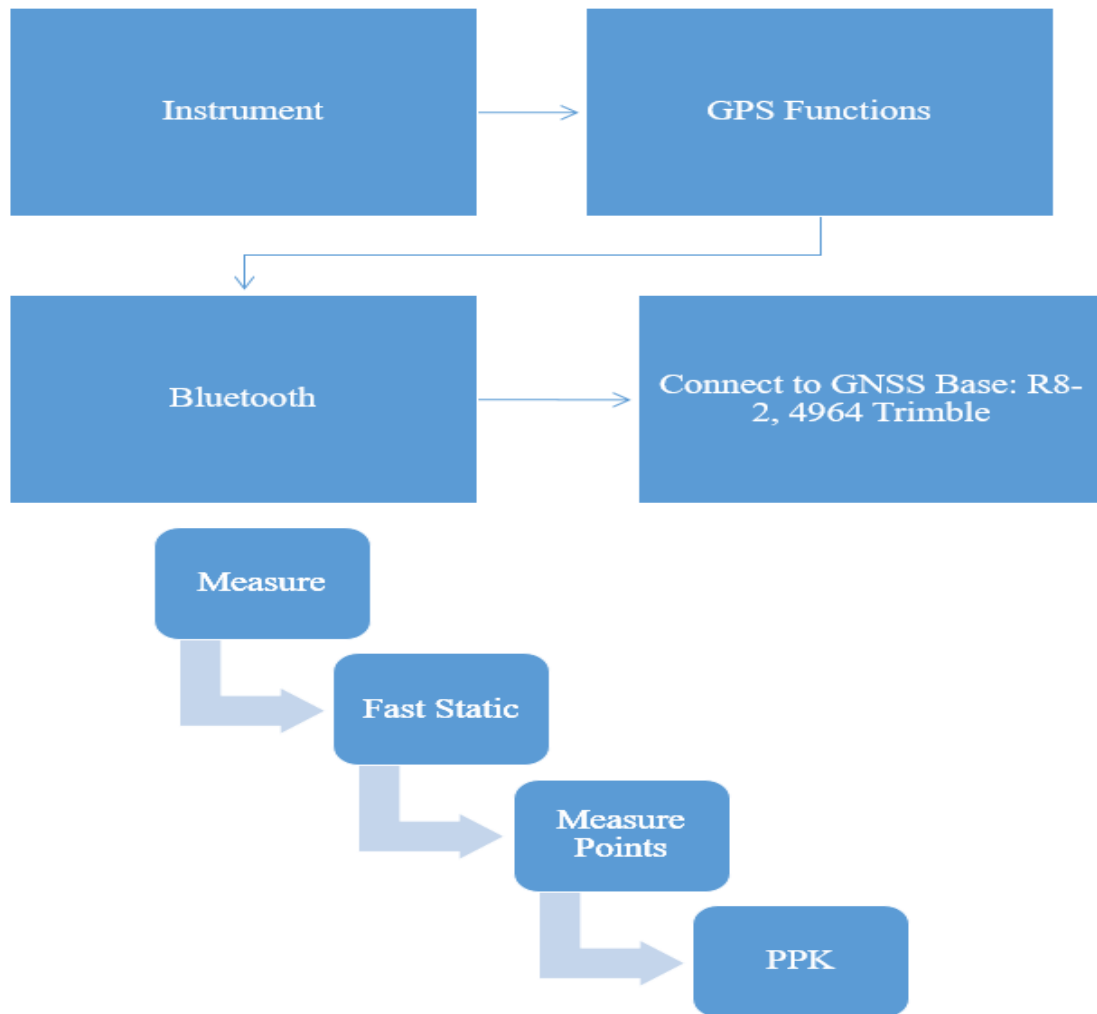


Figure 2: Base and rover connectivity for PPK style of survey

A ppk survey is carried out to map an area where only several centimetres of precision is needed. The data obtained in the field was post-processed to achieve higher precision by using Trimble's Geomatics Office processing software.

2.6 UAV and camera setup specifications



Figure 3: Draganfly X4P UAV and Sony RX100 camera setup (Source: Draganfly, 2017)

2.6.1 Draganfly X4P UAV

The combination of Draganfly X4P UAV and Sony RX100 camera shown in Figure 3, provides high quality imagery due to the UAV's powerful and stable platform. The propellers are made up of carbon fibre and remaining material is plastic; total setup weighing 2.3 kg with the camera. Due to its nimble setup, it can travel at a maximum speed of 50kmph and can withstand up to 25 kmph winds. It is capable to fly up to 2 km above the ground surface but due to the UAV flight regulations in New Zealand, Draganfly X4P was flown under 400 feet. A 14.8V, 5400 mA Lithium-Polymer battery allows the UAV to fly up to 15 minutes, however this is heavily dependent on environmental parameters. It also depends on a vertical launch and landing method, controlled by a custom designed handheld controller.

The Draganfly controller features a direct sunlight viewable touch screen and has wireless linking option. This feature allows the UAV to run in autopilot mode and automated landing is triggered by poor signal or low battery. Draganfly surveyor

software is used to autopilot the aircraft by pre-setting the flight coordinates and path. The only limitation noticed was that the batteries quickly drained from the UAV during its flight, as the wind conditions ranged between 20 kmph to 30 kmph. More power was needed for the UAV to ensure it maintained its course and altitude. The on-board processor with 11 sensors make the Draganfly stable and easy to fly.

2.6.2 Sony RX100

The Sony RX100 camera features a 1.0 type (13.2 x 8.8mm) Exmor CMOS sensor with 20.2 mega pixel and ZEISS Vario Sonnar lens. The 1.0 type sensor is 4 times larger than most compact cameras allowing the user to capture more detail. It has 5 cm – 0.55 m focus range and 10.4 – 37.1 mm focal length, with 3.6x optical zoom and up to 54x digital zoom. RX100 has an internal image processing engine with a still image recommended exposure index ISO sensitivity at ISO 125-6400. The maximum continuous shooting speed of the camera is at 10 frames per second (fps). The camera weighs 240 g with the battery and SD media card with the rechargeable battery NP-BX1 lasting up to 330 shots or 165 minutes of still image photography. The internal sensor and processor assures detailed high sensitivity still images and flawless, clean natural images. The extremely powerful and compact featuring Zeiss stabilized zoom lens can be controlled manually by the Draganfly X4P application mid-flight.

Draganfly X4P and Sony RX100 is a good setup for small scale aerial photography studies. The camera supports digital video downlink, geotagging system, which provides detailed imaging. The camera payload is gyro stabilized and vibration isolated from both the helicopter and camera mounts, to provide clean stills and videos.

2.7 Computer Processing Requirements

The Agisoft Photoscan Pro educational license is available for \$549 USD and allows the use of ground control points, stitching imagery, DEM export, and export a georeferenced orthophoto. Below are the configuration requirements from Agisoft as of April 2017:

Table 1: Agisoft Photoscan Pro configuration requirements (Source: Agisoft, 2017)

Basic configuration (up to 32GB RAM)	Advanced configuration (Up to 64 GB RAM)	Extreme configuration (More than 64 GB RAM)
CPU: Quad-core Intel Core i7 CPU. Socket LGA 1155 (Sandy Bridge, Ivy Bridge or Haswell)	CPU: Six-core Intel Core i7 CPU, Socket LGA 2011 (Sandy Bridge-E)	For processing of extremely large data sets a dual socket Intel Xeon Workstation can be used.
Motherboard: Any LGA 1155 model with 4 DDR3 slots and at least 1 PCI Express x 16 slot	Motherboard: Any LGA 2011 model with 8 DDR3 slots and at least 1 PCI Express x 16 slot	
RAM: DDR3-1600, 4 x 4 GB (16 GB total) or 4 x 8 GB (32 GB total)	RAM: DDR3-1600, 8 x 4 GB (32GB total) or 8 x 8 GB (64 GB total)	
GPU: Nvidia GeForce GTX 780 or GeForce GTX 980 (optional)	GPU: Nvidia GeForce GTX 780 Ti, GeForce GTX 980 or GeForce GTX TITAN X	

The research was conducted on a Windows based platform system as both ArcGIS and Photoscan Pro were readily available at University of Canterbury.

Chapter 3: Research Component

3.1 Fieldwork Methodology

3.1.1 Study Area

The literature review above provides information regarding the August 2012 Te Maari eruptions, introducing the area of study, the ballistic crater field near Ketatahi Hut. A structured approach was necessary to efficiently utilize time and resources, while in the field. Survey site selection, ground truthing, UAV flight operations and data processing constitute 3D modelling. The dimensions of the study site are 100 m², approximately 2 kilometres away from the volcanic vents as shown in Figure 4. This area consists numerous ballistic craters caused by volcanic blocks and features a variation in topographic slope. It can be accessed by going off the Tongariro Alpine Crossing track, just past the Department of Conservation's Ketatahi Hut. The selected study site is away from public access at an elevation of 1370 - 1470 metres. Field preparation involves the development of ground control markers, which is a key step as DEM and orthophoto quality depends on the placement of these targets. The ground control targets were scattered within the survey site and the entire area was divided into two zones. Zone 1 was flown at 40m elevation resulting in 91 images (dataset 1 from UAV flight 1) and zone 2 was flown at 20m elevation resulting in 145 images (dataset 2 from UAV flight 2). These datasets from the UAV were used to produce orthophotos and DEM's in Agisoft Photoscan Pro photogrammetric SfM software.

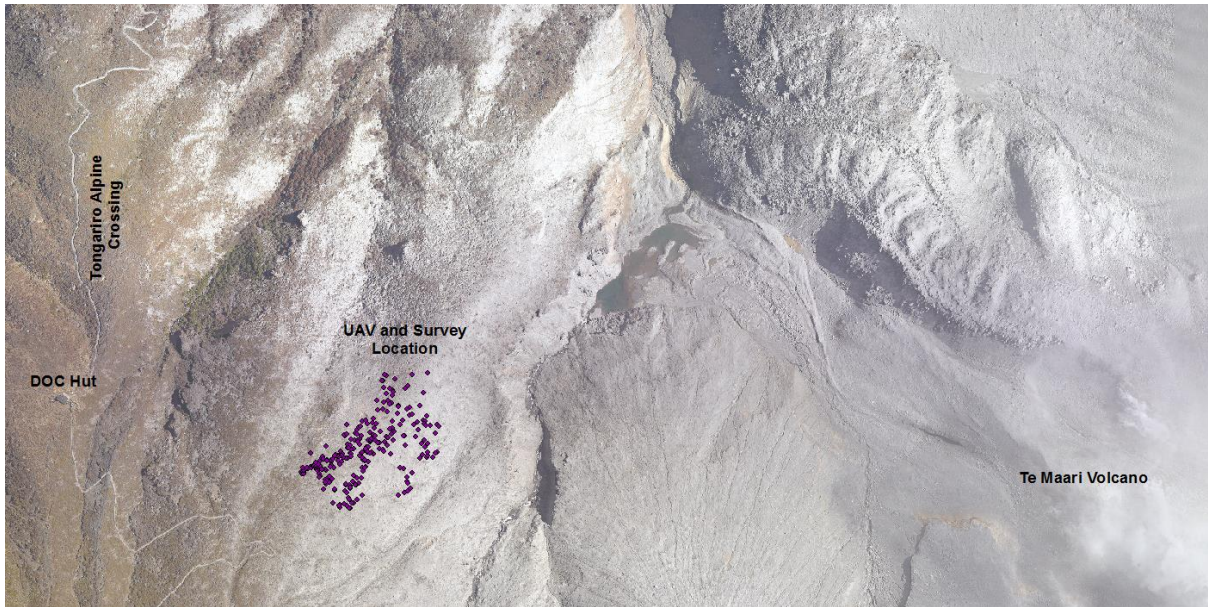


Figure 4: Selected study site within the August 2012 volcanic ballistic crater field

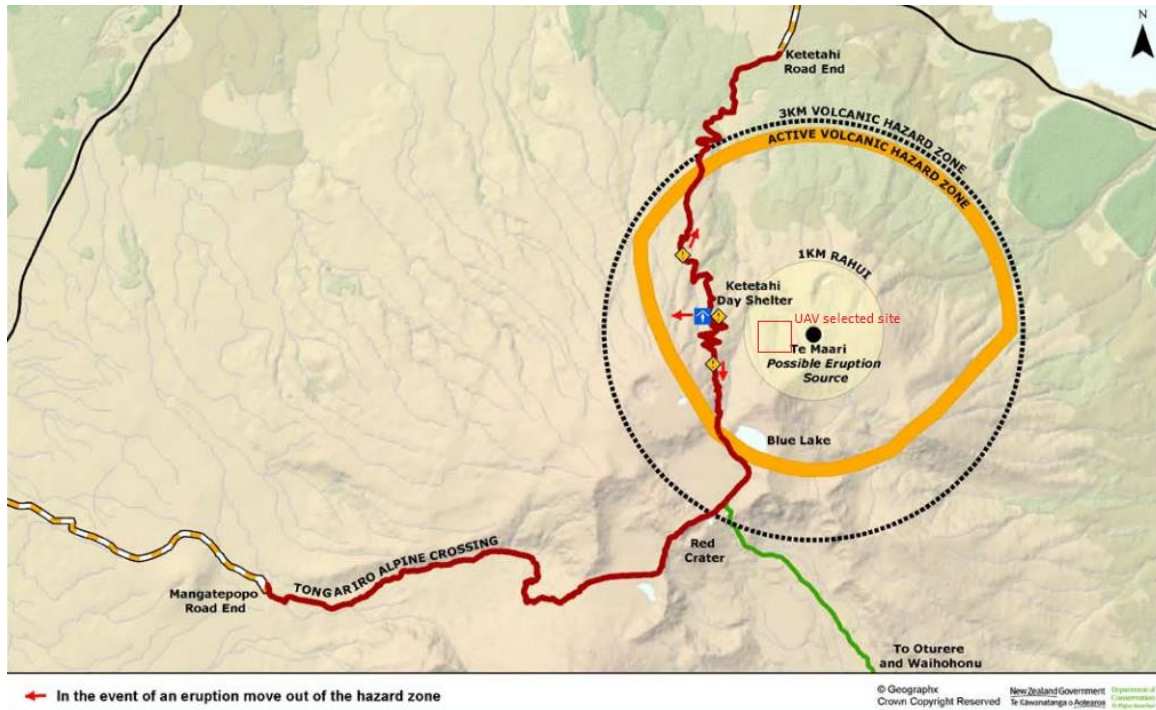


Figure 5: Volcanic hazard zone radius of future Te Maari eruption (Source: Department of conservation, NZ)

The orthophotos and DEM's generated from the software were used to identify and analyse the craters four years post 2012 eruptions. A point score model was built to identify the craters using this dataset. Various parameters such as crater size, crater shape, surrounding vegetation, shadow, nearby blocks and presence of debris apron were used to assist in building the model.

3.1.2 Draganfly UAV Flight and GCPs

Aerial photogrammetry was conducted on 14th January 2016, by flying the Draganfly X4P UAV at 40 metre and 20 metre elevations. The duration of both the UAV flights lasted 13 minutes taking a total of 236 pictures using Sony RX100 camera. Flight 1 comprised a total of 91 images spanning 7 minutes at 40 metres elevation above ground surface, with wind blowing at 25kmph. Flight 2 comprised a total of 145 images spanning 6 minutes of flight time at 20 metres elevation above ground surface at similar wind conditions. The study area was also ground-truthed using GNSS R8 equipment on separate occasions (3rd, 5th Dec 2015 and 14th January 2016).

Draganfly Surveyor software is used to autopilot the UAV by pre-setting the coordinates. The software saves the flight path and records the northing, easting and elevation data of ground images in log files, which can be later converted to comma delimited format.



Figure 6: GCP target design for identification purpose on ground surface

The UAV was always flown below 120 m at Tongariro National Park and within line of sight because of the project requirements and UAV regulations flight requirement in NZ. A total of 10 GCP targets were used in this project for each flight. Figure 6 shows the design of the GCP targets used in this project. Figure 7 shows how the ground control targets look from the UAV at 20m elevation and 40m elevation above the ground surface. Although 10 GCPs were used for each flight, only 6 to 8 GCPs were used for proper orientation and geo-referencing while generating an orthophoto and DEM. Table 2 provides some examples of ground truthing data collected from the field.

Table 2: Some examples of ground truthing data collection of GCPs and natural features

Name	Northing	Easting	Elevation
GCP2-Area1	5667774.16512	1829728.42331	1460.27573
GCP3-Area1	5667767.6849	1829761.9601	1446.98546
GCP4-Area1	5667838.25136	1829792.77136	1430.35457
GCP1-Area2	5667870.25394	1829792.96836	1428.11795
GCP5-Area2	5667835.48605	1829800.41406	1433.63587
GCP6-Area2	5667846.46113	1829784.84819	1435.14811
naf1redboulder	5667853.10464	1829845.88887	1411.96404



Figure 7: GCP targets from 20m elevation (top) and 40m elevation (bottom) taken from Draganfly X4P UAV

The 10 GCP targets were thoughtfully placed within the survey site for flight 1 so that they cover the entire area uniformly, especially the middle and corner regions. This allows the Photoscan Pro software to interpolate the position of the GCP targets without major warping. The other advantage of creating easily visible GCP targets is to allow the software to automate GCP placement and reduce the error. The GCP targets for this project were made up of flat synthetic non-shiny material painted in black with a unique number on it. It allows the UAV to easily pick up the ground target at elevations greater than 50 metres.

3.1.3 Ground Truthing using Trimble GNSS R8 and TSC₃ Controller

Ground truthing is a commonly practiced method to measure field data in geology, geography and survey related studies (Fitzgerald, 2014). It is a measure of comparing remotely sensed and calculated field data against data measured in the field. The study area was first surveyed on 3rd and 5th December 2015, using a Trimble GNSS R8 system and a Trimble TSC3 controller. The weather was inconsistent and the survey was hampered by visibility issues on both the days. However, the objective was to collect information on as many volcanic craters as possible within the selected area. Figure 8 shows some examples of ballistic craters that were caused by 2012 Te Maari volcanic eruptions.

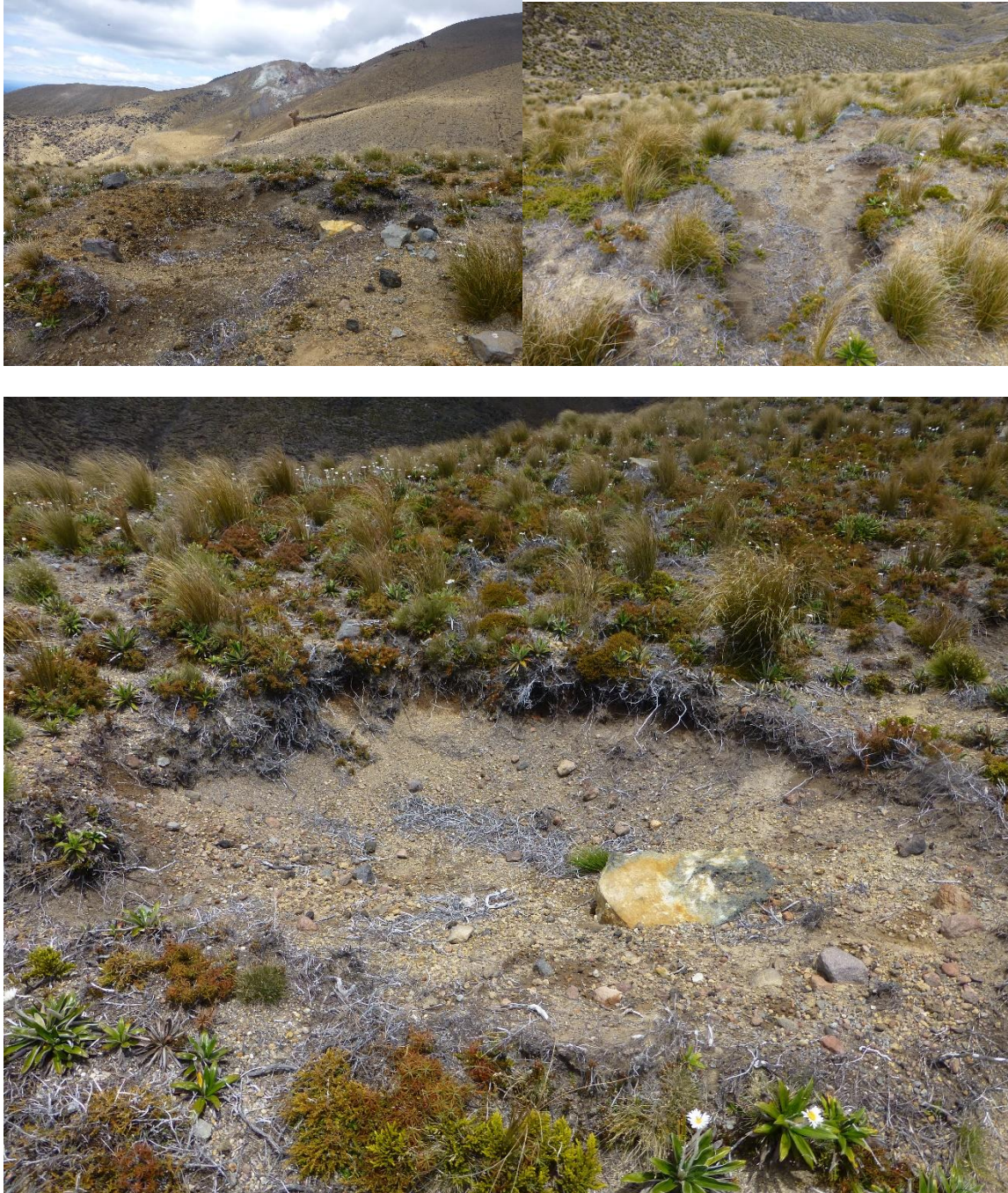


Figure 8: Range and variations of volcanic craters at Te Maari eruption site (images taken in 2016)

Some natural features and point of interests had also been captured with their northing, easting and elevation data that can be confidently identified on the aerial images. Fast static survey style is used to shorten the observation and capture time due to time restrictions. A horizontal and vertical error of ± 5 mm is associated with fast static surveys, however accuracy and reliability is affected by satellite reception,

atmospheric conditions and obstructions (Bakula, 2013). A total range of 8 to 14 satellites were available to the GNSS R8 during the ground truthing process.

3.2 Agisoft Photoscan Pro workflow

To ease the workload of the processor, the Draganfly's flight 1 and flight 2 images were processed separately in Agisoft photoscan pro software. Flights 1 and 2 consist of 91 and 145 images respectively, with NZTM2000 as its projected coordinate system. Figure 9 outlines the workflow chart followed to create a digital elevation model in Agisoft and Figure 10 shows the variation of ground surface after each workflow step.

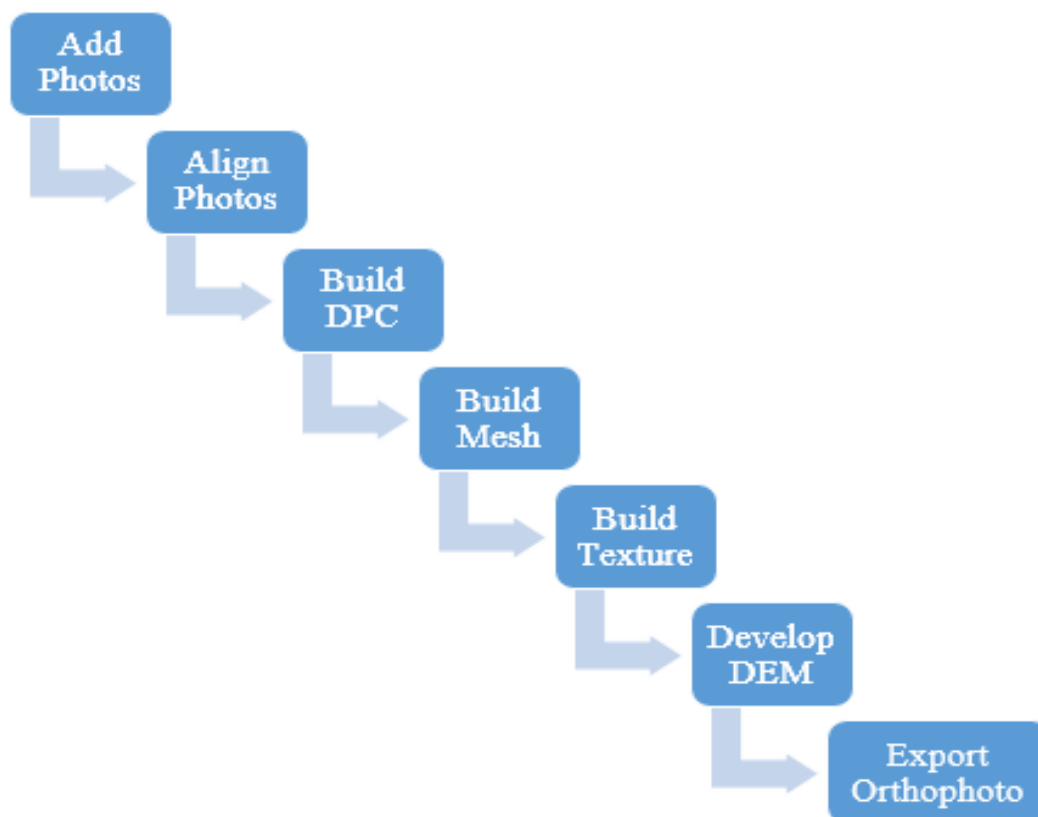


Figure 9: Photoscan Pro SfM workflow to create digital elevation model

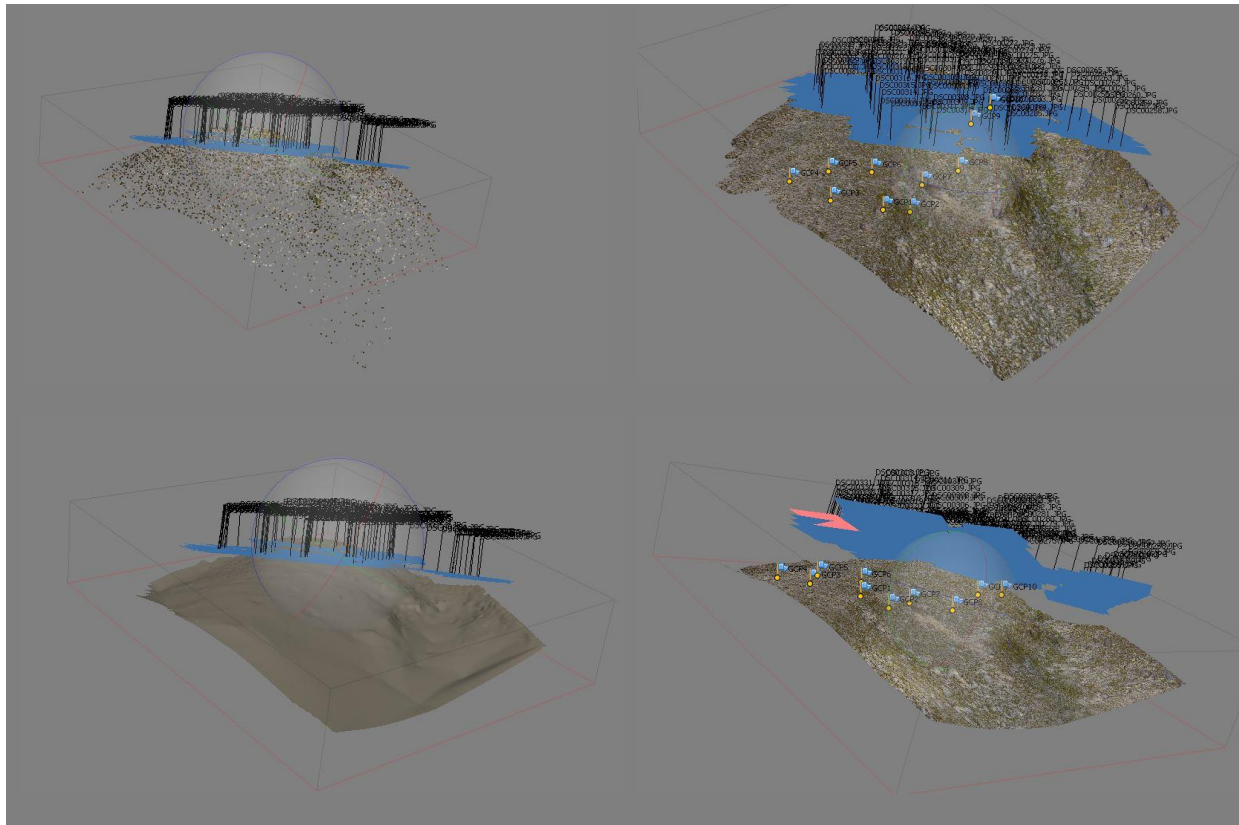


Figure 10: Flight 1 imagery dataset (91 images) a) post image-alignment (top left) b) dense point cloud (top right) c) post build-mesh (bottom left) d) post build texture (bottom right)

All the flight 1 (91 images) are inserted using 'add photos' option under workflow menu. The UAV coordinates are uploaded into the software using the reference tab; selecting NZTM2000 as its projected coordinate system. The photos are aligned with accuracy at its highest setting and using the drone coordinates file as reference for pair selection. This allows the software to align photos by detecting points, selecting pairs and matching points automatically to create Figure 10a. A medium quality dense point cloud (DPC) is generated by loading the photos and reconstructing the depth of the images, shown in Figure 10b. A mesh is built by analysing the DPC and calculating the vertex colours, shown in Figure 10c. Build texture feature parameterizes texture atlas, calculates colour correction and blends textures to create Figure 10d. A similar workflow process is followed for flight 2 (145 images) to

develop Figure 11. Ultimately, SfM workflows from UAV imagery datasets 1 and 2 produce two DEM's with elevations ranging from 1397 to 1462 metres.

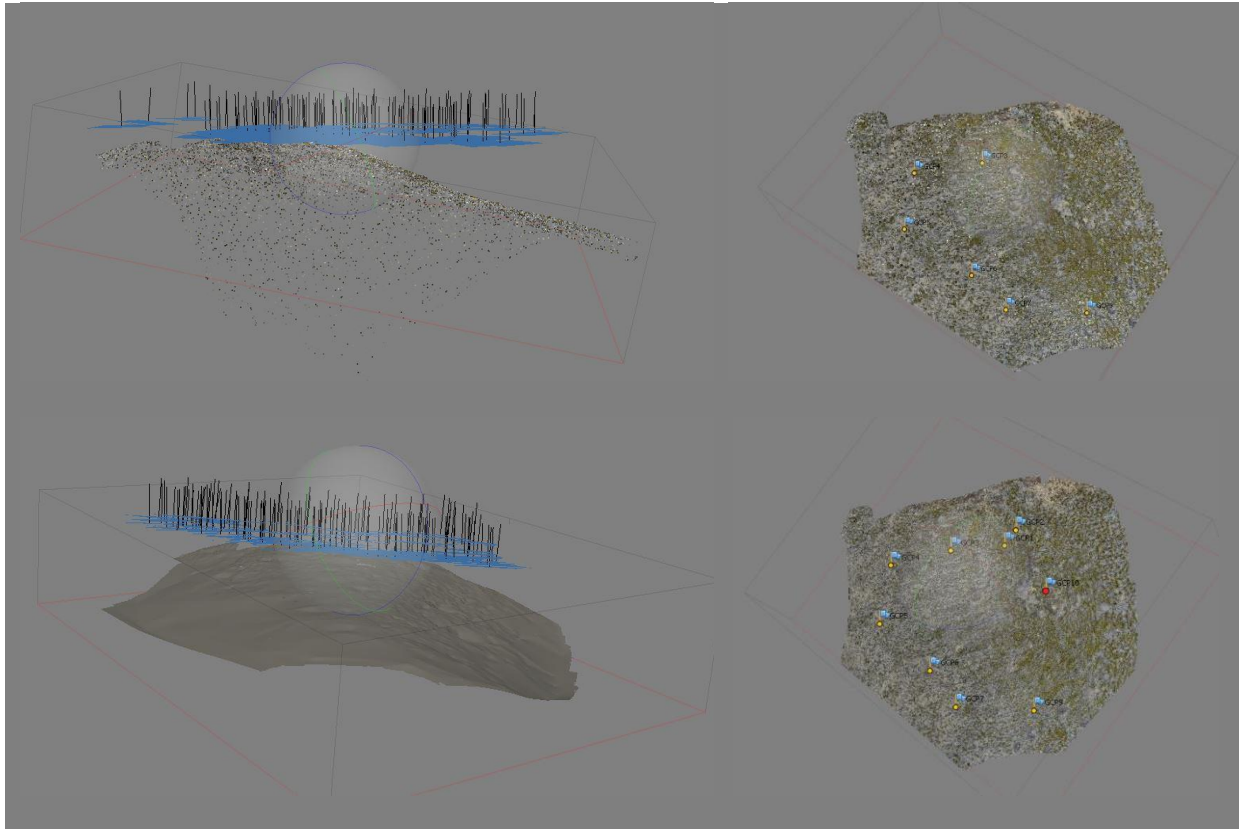


Figure 11: Flight 2 imagery dataset (145 images) a) post image-alignment (top left) b) dense point cloud (top right) c) post build-mesh (bottom left) d) post build texture (bottom right)

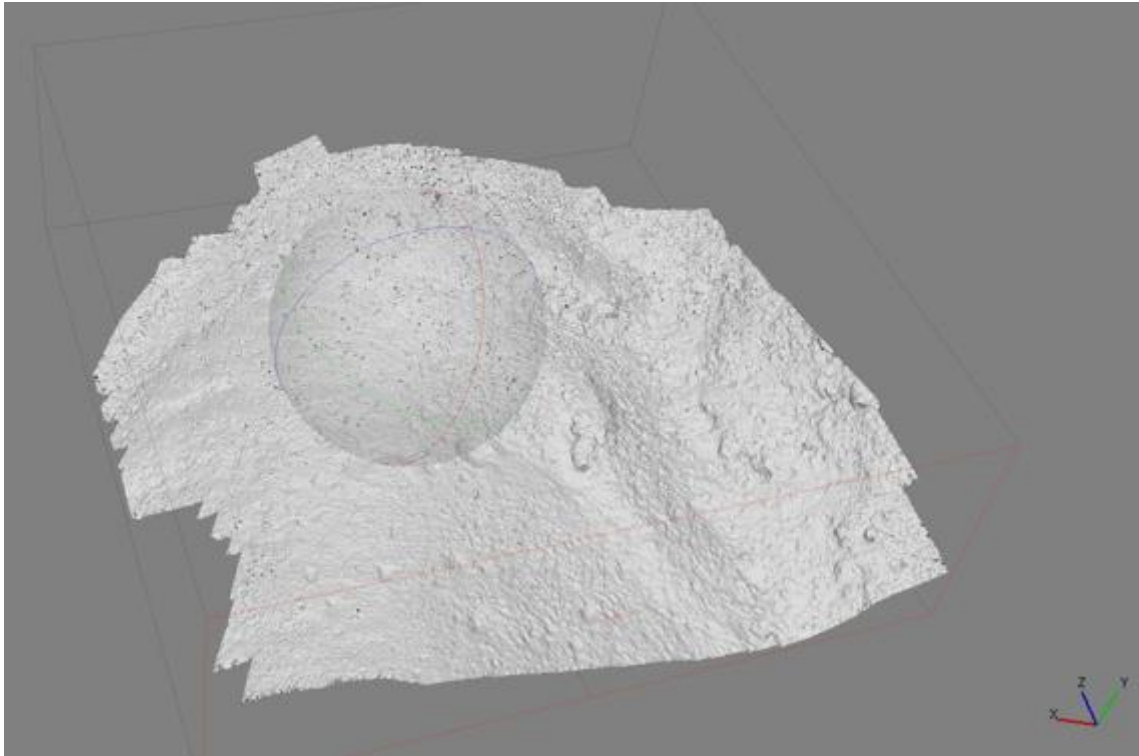


Figure 12: DEM of imagery 1 dataset in SfM Photoscan Pro software

Ground-truthing data collected by Trimble R8 systems is used in SfM software to generate higher accuracy 3D models. Figure 12 shows the DEM model of flight 1 UAV imagery dataset in SfM software. The DEM models are exported into ArcGIS software and section 4.2 explains on how it aids to build a volcanic crater identification model.

Figures 13-19 show the user-friendly reports generated by Agisoft Photoscan Pro software of camera locations, GCP locations and image overlap for flight 1 and flight 2 datasets.

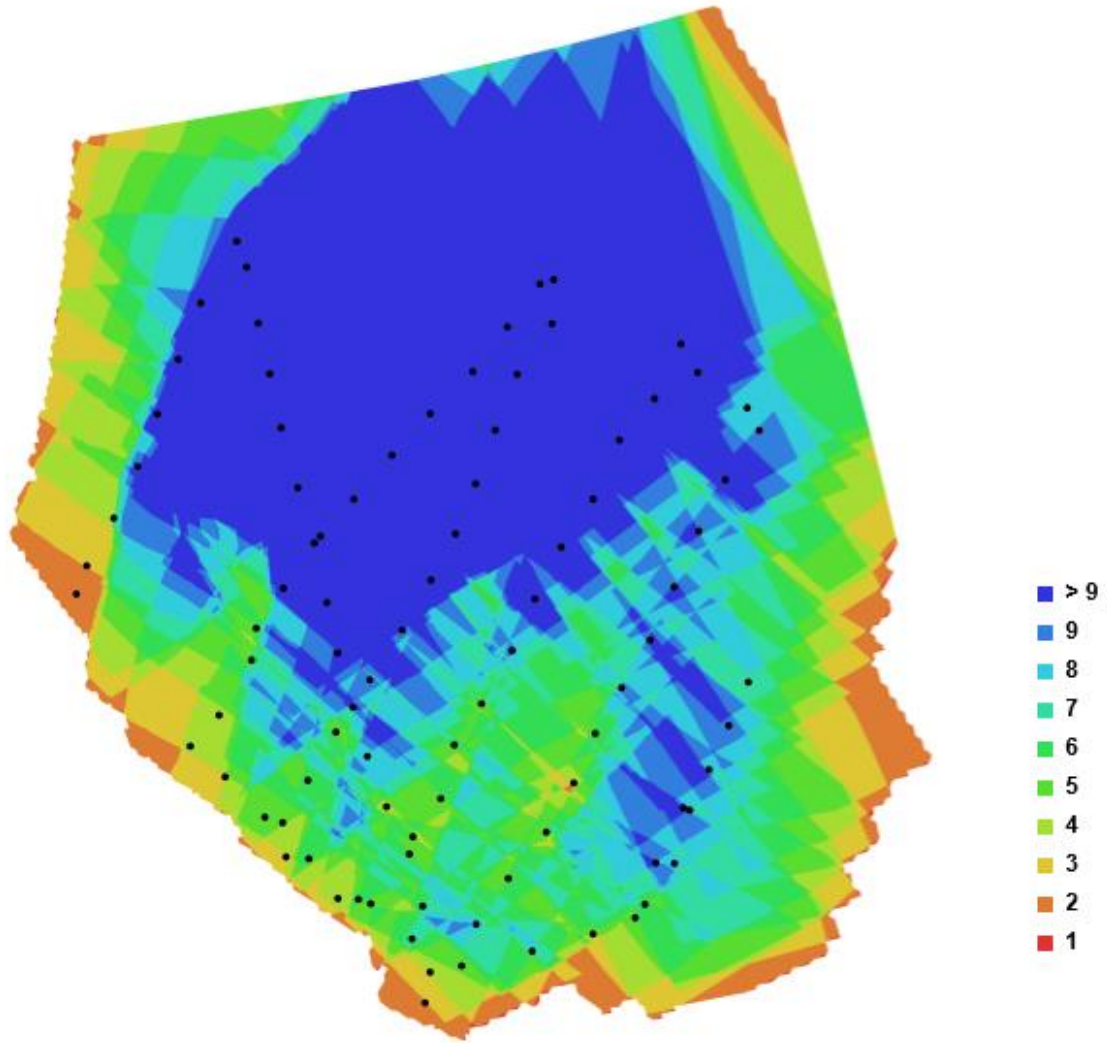
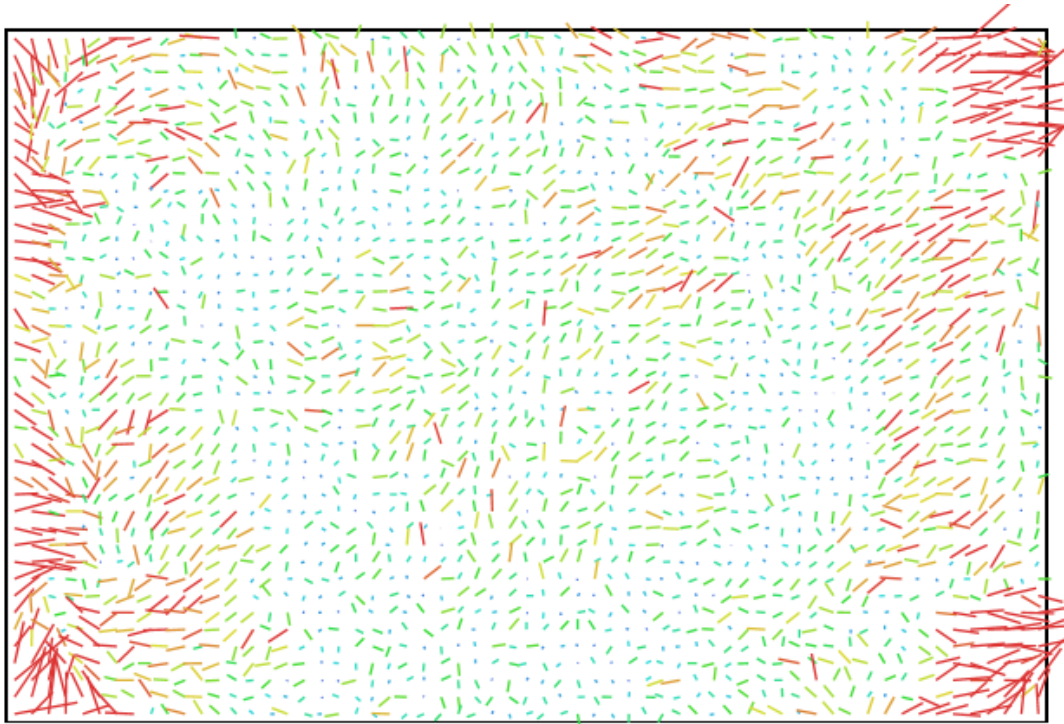


Figure 13: Camera locations and image overlap of flight 1 dataset

Number of images:	91	Camera stations:	91
Flying altitude:	41.9895 m	Tie-points:	17688
Ground resolution:	0.0102593 m/pix	Projections:	90676
Coverage area:	0.0253114 sq km	Error:	0.995767 pix

Camera Model	Resolution	Focal Length	Pixel Size	Precalibrated
DSC-RX100M3 (8.8 mm)	5472 x 3648	8.8 mm	2.41228 x 2.41228 um	No

Figure 14: SfM resolution survey details of flight 1 dataset



1 pix

DSC-RX100M3 (8.8 mm)

Type:	Frame	K1:	-0.000510613
Fx:	3760.69	K2:	0.0126408
Fy:	3760.69	K3:	-0.0153248
Cx:	2739.3	K4:	0
Cy:	1829.65	P1:	0
Skew:	0	P2:	0

Figure 15: Image residuals for DSC-RX100M3 (8.8 mm) camera calibration of flight 1 dataset

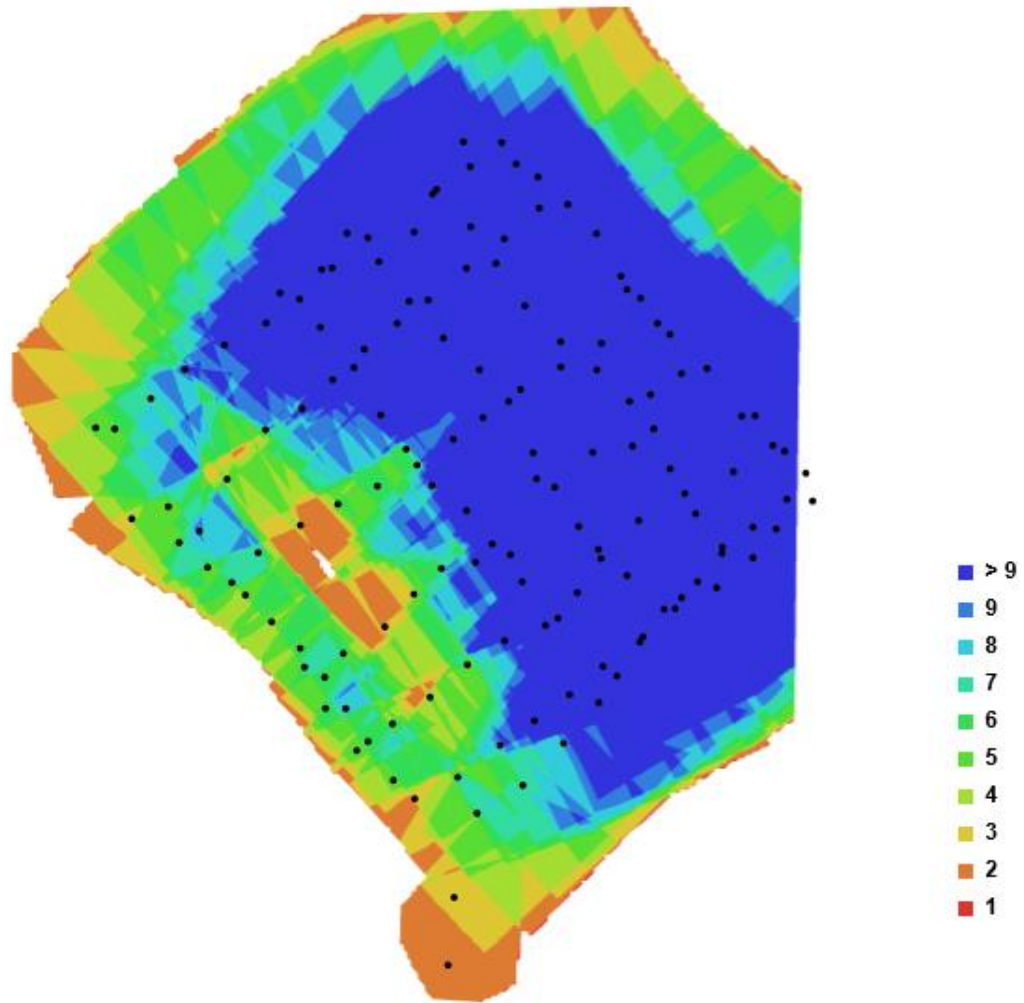
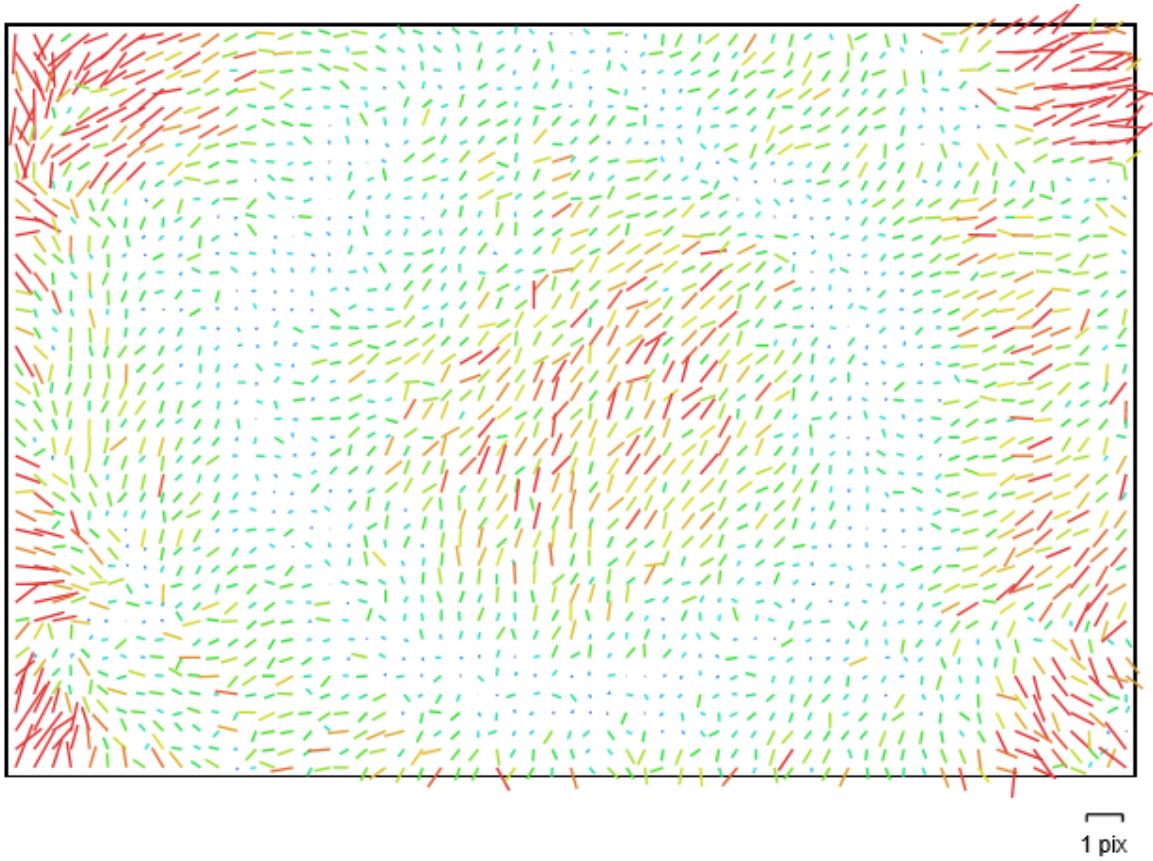


Figure 16: Camera locations and image overlap of flight 2 dataset

Number of images:	145	Camera stations:	145
Flying altitude:	22.4695 m	Tie-points:	22401
Ground resolution:	0.00541427 m/pix	Projections:	131231
Coverage area:	0.00783175 sq km	Error:	1.2133 pix

Camera Model	Resolution	Focal Length	Pixel Size	Precalibrated
DSC-RX100M3 (8.8 mm)	5472 x 3648	8.8 mm	2.41228 x 2.41228 um	No

Figure 17: SfM resolution survey details of flight 2 dataset



DSC-RX100M3 (8.8 mm)

Type:	Frame	K1:	-0.00050724
Fx:	3792.67	K2:	0.0180949
Fy:	3792.67	K3:	-0.0211467
Cx:	2743.96	K4:	0
Cy:	1831.89	P1:	0
Skew:	0	P2:	0

Figure 18: Image residuals for DSC-RX100M3 (8.8mm) camera calibration of flight 2 dataset

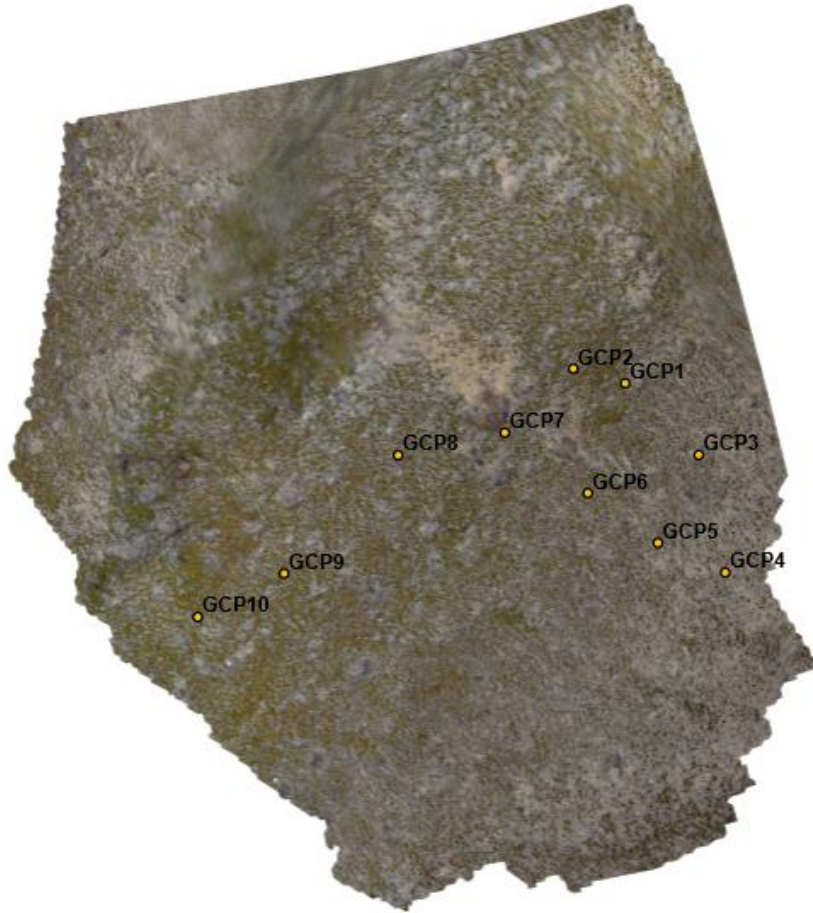


Figure 19: Ground control point locations of flight 1 dataset

Table 3: GCP locational error values of flight 1 dataset

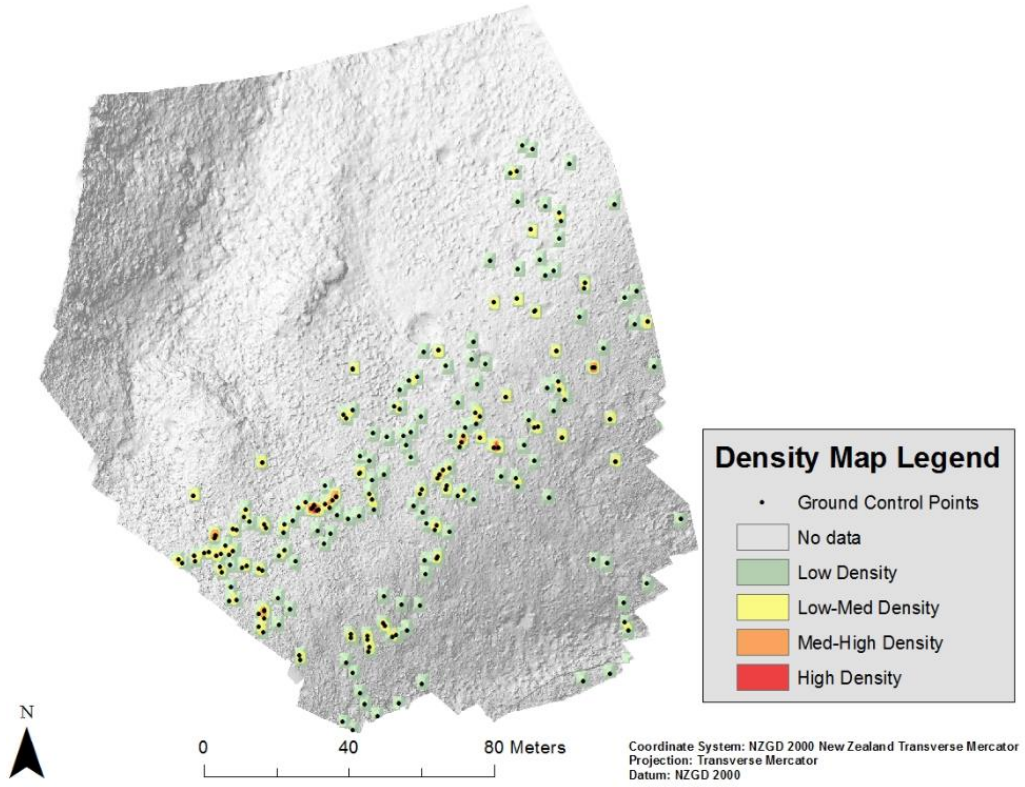
Marker	X Error (m)	Y Error (m)	Z Error (m)	Error (m)	Projections	Error (pix)
GCP9	0.033981	-0.061530	-1.262307	1.264262	9	0.645714
GCP8	0.082108	0.242281	-0.156551	0.299917	14	0.804037
GCP10	-0.037750	-0.544345	0.451467	0.708209	5	0.558475
GCP7	0.007553	0.101364	0.684440	0.691946	14	0.907087
GCP6	-0.103025	-0.313758	0.316529	0.457437	8	0.378020
GCP1	-0.003608	0.080830	1.085368	1.088379	10	0.450291
GCP3	-0.052933	-0.039569	0.261840	0.270051	6	0.538965
GCP5	-0.193829	-0.262175	-0.413104	0.526270	6	0.630085
GCP4	-0.276957	-0.123505	-0.795682	0.851510	4	0.718317
Total	0.123416	0.249356	0.702436	0.755530	76	0.680959

Chapter 4: Results

4.1 Role of Geographic Information Systems (GIS) and SfM for volcanic crater modelling

GNSS R8 survey equipment used to capture 289 ground control points is converted into a shape file and added into ArcMap software. This file contains information regarding easting, northing and elevation of different sized craters within the ground-truthed area. The two DEMs generated from Agisoft Photo Scan Pro software are also added into ArcMap as raster images. The hill-shade spatial analyst tool creates a shaded relief raster from a raster images. The output raster only considers a local illumination angle as the model shadows option is disabled. An optimized hotspot spatial analysis tool creates a map of statistically significant hot and cold spots using the GNSS ground control points to produce optimal results. The statistically significant clusters of high values represent hot spots and low values represent cold spots as shown in Figure 20. The size of the clusters represents the total number of craters available in a certain spot.

Density Map of Ground Control Points at Te Maari



Optimised Hotspot Analysis of GNSS ground control points at Te Maari

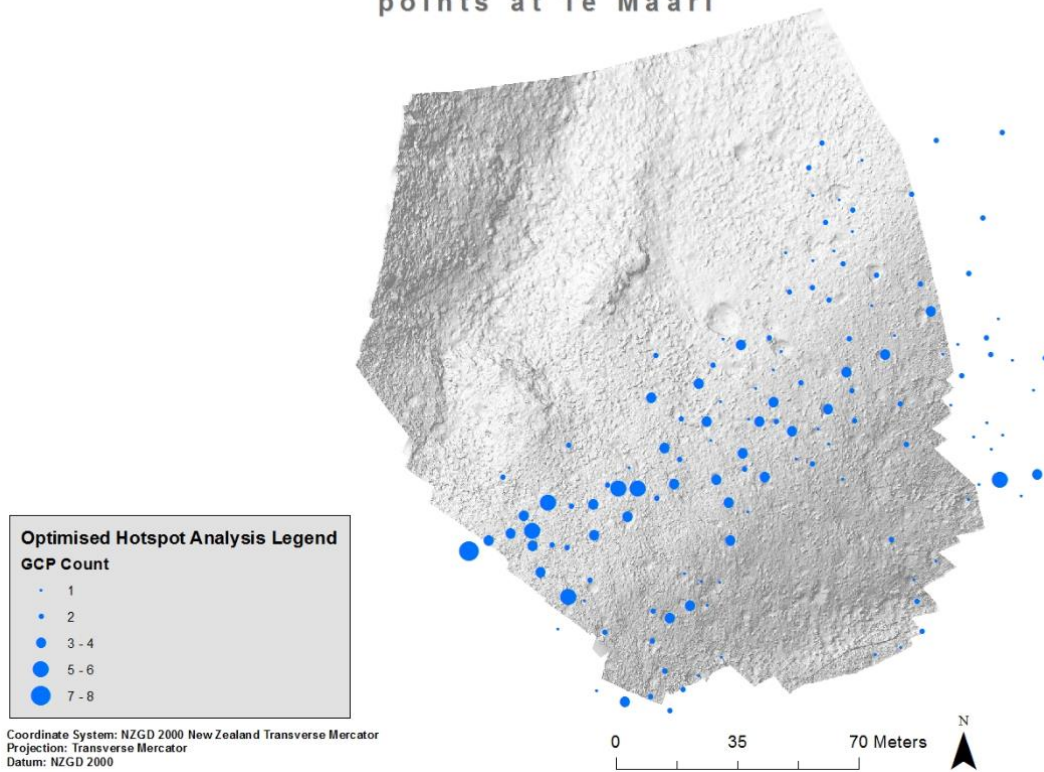


Figure 20: a) Density pattern of GCPs (top) b) Optimised hotspot analysis of GCPs

The density pattern is developed using an Empirical Bayesian Kriging interpolation method that accounts for the error in estimating the underlying semi-variogram through repeated simulations.

4.2 Identifying craters using SfM

A point score model is developed in ArcMap to accurately identify volcanic craters on the ground surface using a standardised model. Volcanic craters can be difficult to identify visually especially four years post 2012 Te Maari volcanic eruptions due to vegetation growth and natural processes effecting the landscape. Hence, key parameters such as crater shape, size, vegetation, shadow, block, debris apron and DEMs, generated by Agisoft are used to build a standardised model to identify the volcanic craters. The morphology of volcanic craters at Te Maari consists of debris aprons caused by disposed material due to the collision. Burnt or broken vegetation roots, the presence of a block within the crater or nearby, crater shape and shadow of the slope from direct sunlight help in building the crater identification process.

Table 4: Point score model to identify volcanic craters

OBJECTID *	Shape *	Id	Vegetation	Shadow	Block	Debris_Apr	DEM	Agisoft	Crater_Shape
1	Point	1	y	y	y	y	y	y	round
3	Point	2	y	y	n	y	y	y	irregular
4	Point	3	y	n	y	y	y	y	irregular
6	Point	4	y	y	n	y	y	y	round
7	Point	5	y	y	y	y	y	y	round
8	Point	6	y	y	y	y	y	y	round
9	Point	7	y	y	n	y	y	y	round
10	Point	8	y	y	y	y	y	y	irregular
11	Point	9	y	y	y	y	y	y	irregular
12	Point	10	y	y	y	y	y	y	irregular
13	Point	11	y	y	y	y	y	y	irregular
14	Point	12	y	y	y	y	y	y	round
15	Point	13	y	y	y	y	y	y	round
16	Point	14	n	y	y	y	y	y	irregular
17	Point	15	y	y	n	y	y	y	round
18	Point	16	y	y	y	y	y	y	round
19	Point	17	y	n	y	y	y	y	round
20	Point	18	y	y	y	y	y	y	round
21	Point	19	y	y	y	y	y	y	round
22	Point	20	y	n	y	y	y	y	round
23	Point	21	y	y	y	y	y	y	irregular
24	Point	22	y	y	y	y	y	y	round
25	Point	23	y	y	y	y	y	y	round
26	Point	24	y	y	y	y	y	y	round
27	Point	25	y	n	y	y	y	y	round
28	Point	26	y	n	n	y	y	y	round
29	Point	27	y	n	y	y	y	y	round
30	Point	28	y	n	n	y	y	y	round
31	Point	29	y	n	y	y	y	y	round
32	Point	30	y	n	y	y	y	y	round
33	Point	31	y	y	y	y	y	y	round
34	Point	32	y	y	y	y	y	y	round
35	Point	33	y	y	y	y	y	y	round
36	Point	34	y	y	y	y	y	y	round
39	Point	35	y	y	y	y	y	y	round
40	Point	36	y	y	y	y	y	y	irregular
41	Point	37	y	y	y	y	y	y	round
42	Point	38	y	y	y	y	y	y	round
43	Point	39	y	n	y	y	y	y	round
45	Point	40	y	y	n	y	y	y	round
46	Point	41	y	n	y	y	y	y	round
47	Point	42	y	y	y	y	y	y	irregular

The orthophoto DEM's generated by Draganfly imagery is extremely helpful to aid the identification process. The three-dimensional visuals available from Agisoft photo scan pro software is used as a final parameter in the model to accurately identify a crater as it allows the user to zoom in to a location for detailed inspection. Debris apron, shadows, burnt vegetation and location of blocks are the other parameters used to identify crater locations. The shape of craters on the ground surface aids the user in crater identification process. A total of 135 were successfully identified using this method within the 100 m² survey site.

4.3 GNSS versus DEM generated measurements

There will always be a difference in elevation measurement between GNSS measured elevation profile and a DEM generated elevation profile due to various human and computational reasons. Accuracy of measurements depends upon atmospheric effects, multipath effects and satellite geometry. Position Dilution of Precision (PDOP) indicates the quality of the geometry of the satellite constellation (Langley, 1999). The computed or measured data depends on which satellites are used for measurement. A lower PDOP provides a better measurement as there is a greater angle between the satellites. Poor satellite geometry causes high PDOP value and large errors in the measurement. GNSS elevation dataset has GPS measured elevation values of the volcanic craters obtained by ground-truthing the survey site. A new set of different elevation values for the same volcanic craters are generated on the raster DEM file, using geoprocessing tools in ArcMap. The two different sets of elevation values; i) GPS measured or GNSS elevation dataset and ii) DEM elevation dataset, are plotted against each other as shown in Figure 21.

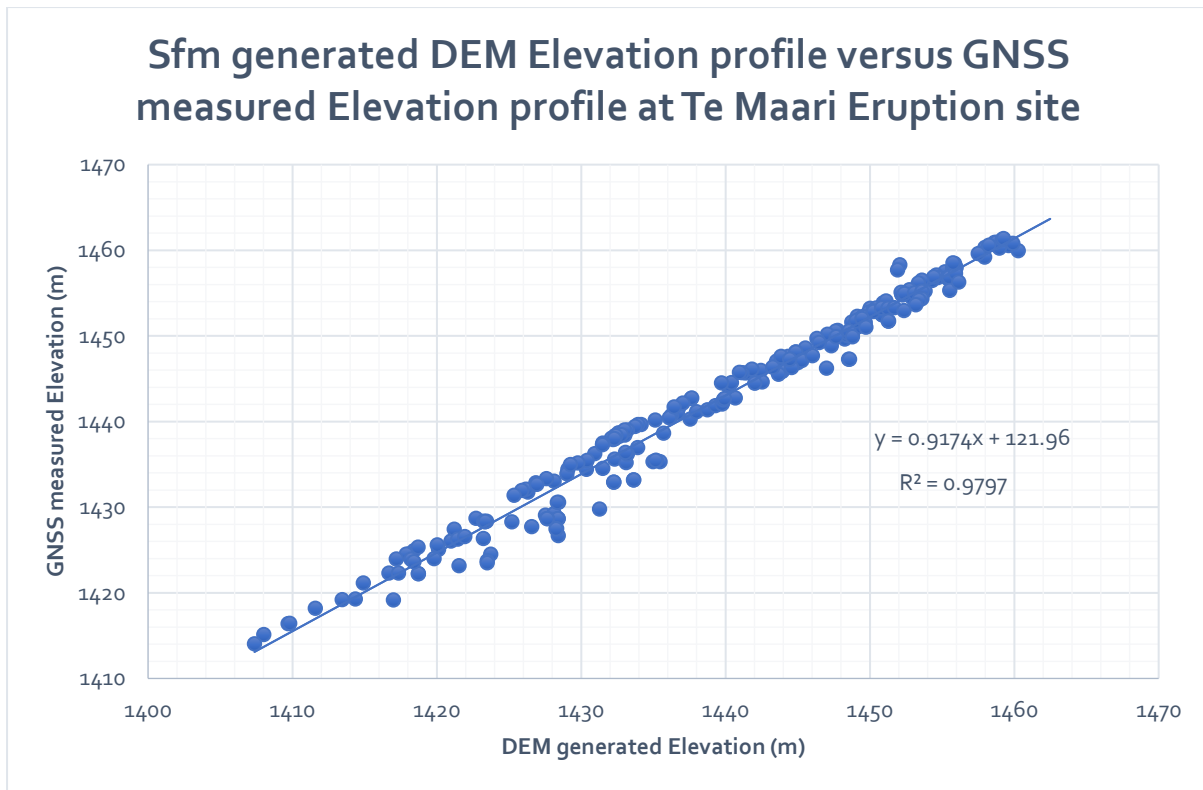


Figure 21: Sfm generated DEM elevation profile versus GNSS measured elevation profile at Te Maari

R-squared, also known as coefficient of determination is a statistical measure on determining how close the data is to the fitted regression line. The model has a gradient of 0.91 and 0.97 as R-squared value.

A statistics model proposed by (Navidi, 2006) was developed further to include bias error and DEM error, to calculate expected values of the elevation profile. Bias of the measurement is defined as the difference between the average and true value of measurements. DEM error is the error generated by the elevation values obtained from the model. To calculate the expected elevation values, the following equation is used:

$$E_v = M_v \pm \text{Bias} \pm \text{DEM Error}$$

Where E_v is the expected elevation value, M_v is the measured GNSS elevation value, bias of the model is 4.56 metres and the total DEM error generated is 5.33 metres. Figure 22 shows the maximum and minimum value range of expected

elevation values for each GNSS recording obtained from the survey site. A total of 298 observations were recorded during the ground truthing process.

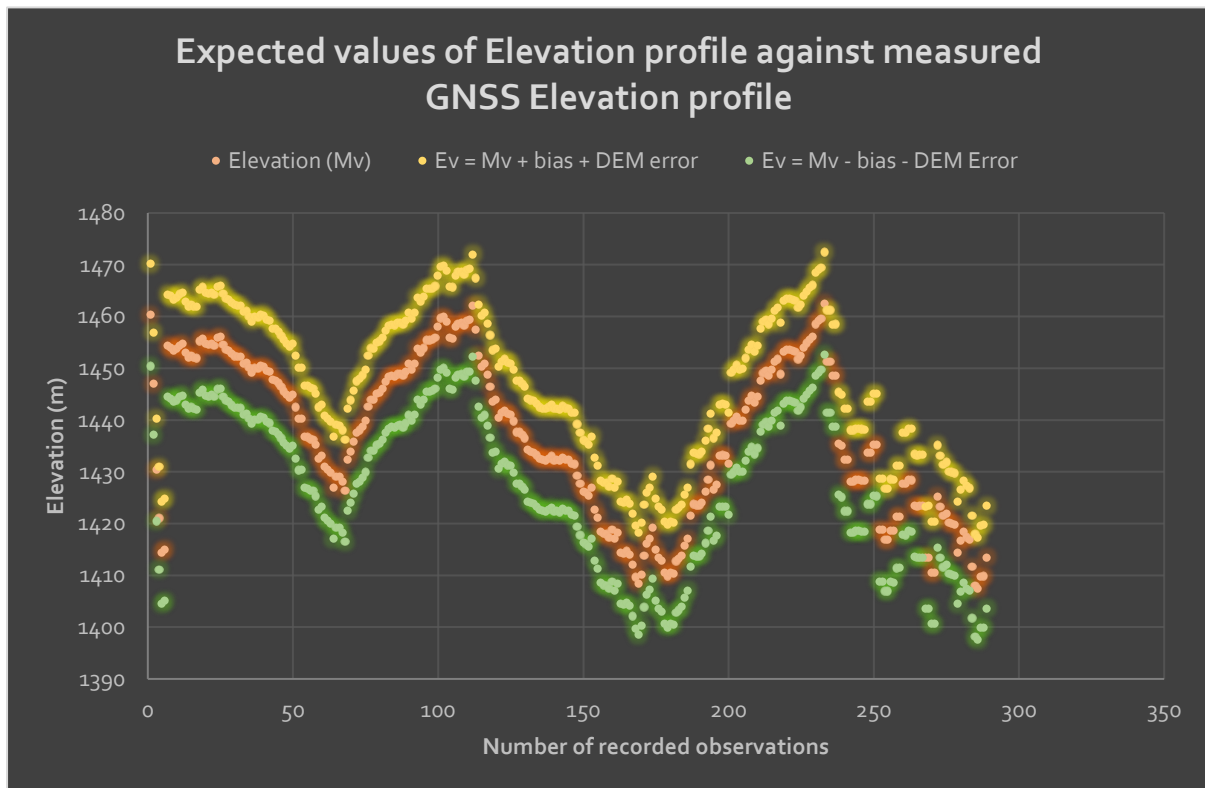


Figure 22: Expected values of elevation profile against measured GNSS elevation profile

The concept of accuracy versus precision, explained by (Viera & Garrett, 2005) is critical to understand the errors of ground control points of GNSS measurements. By the application of this concept, it was identified GCP count and RMS error are ways to identify GCP error. Manual selection of GCP's in Agisoft reduces the RMS error. Flight 1 and flight 2 datasets produced 0.75m and 0.51m RMS error. Precision of the ground control points is 15.05 m, and it is generated by calculating standard deviation of the model.

4.4 Image Resolution and its effect on DEM

The Draganfly X4P UAV was used to take two sets of imagery datasets for the survey region. Flight 1 dataset captured a pixel density (resolution) of 118 pixels per centimetre (PPCM) to produce a DEM using Agisoft Photoscan Pro photogrammetric software. Section 3.2 already covers the process of producing a DEM to identify ballistic impact volcanic craters. Adobe Photoshop software was used to manually lower the resolution of flight 1 imagery dataset from 118 ppcm to 70 ppcm. The new set of 70 ppcm images were uploaded into Agisoft Photoscan Pro to produce a lower resolution DEM for the same location. A similar process outlined in Section 4.2 was followed to manually identify volcanic craters. Figure 23 shows an orthophoto of the lower resolution flight 1 dataset.

A total of 101 craters were identified using the 70 ppcm images when compared to 135 craters using the 118 ppcm images. This is a significant result even though the same methods from section 4.2 were followed for identifying craters. As the resolution of images decreases to 70 ppcm, distortion occurs and the quality of the DEM decreases resulting in a difference of 34 doubtful crater locations. The resolution of the images is dependent on the UAV flight, atmospheric conditions and technical equipment used to capture imagery. The resolution of images is directly proportional to the quality of DEM produced in the photogrammetric software.

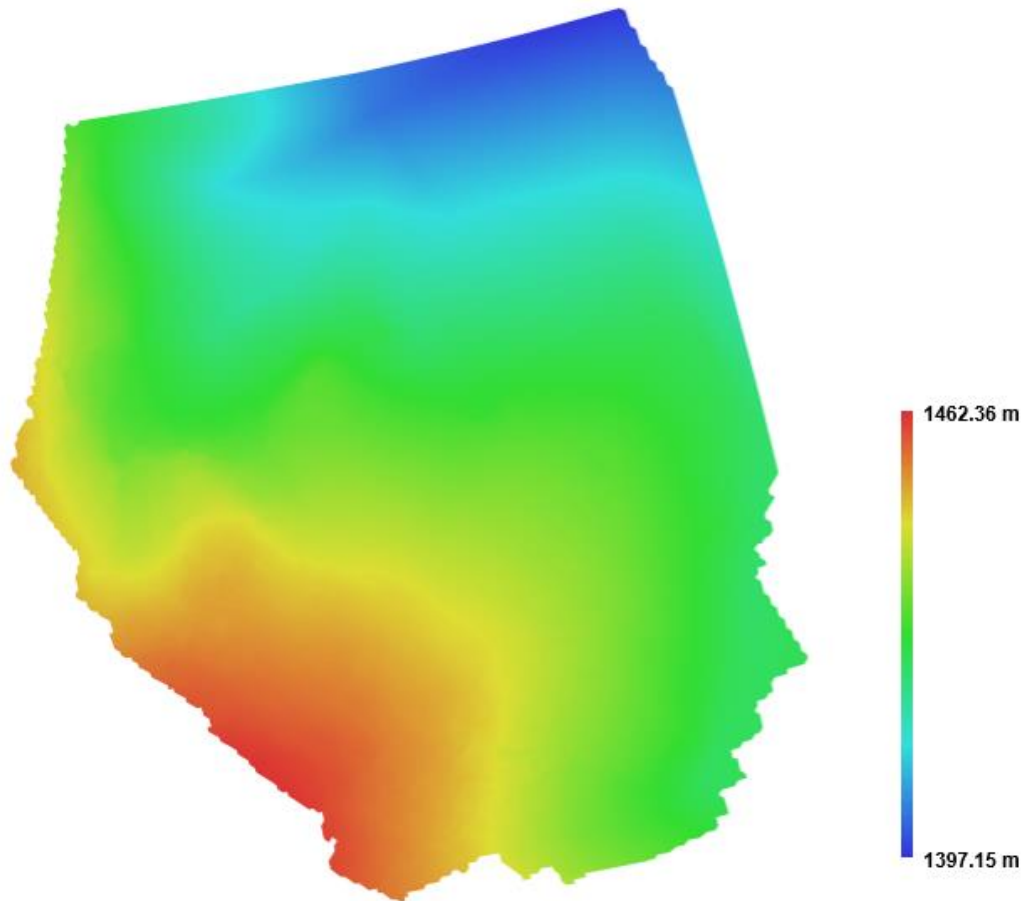


Figure 23: Orthophoto of low resolution dataset 70ppcm

Chapter 5: Discussion

5.1 Explanation of Error Map

Figure 24 shows the elevation profile maps generated by Agisoft Photoscan Pro software with highest elevation at 1462 metres (red) and lowest elevation at 1397 metres (blue). Imagery 1 UAV dataset has a resolution of 118 ppcm. An elevation profile error map is the difference in elevation between GNSS error measurements and DEM error measurements. Areas with the highest amount of error (green) and the areas with least error (pink) are shown in Figure 25. Several potential reasons exist for the error such as, a) lack of overlap between photographs, b) lack of contrast and poor constrain between features (not linking properly), c) poor recording of rapid ground acceleration, d) Error in a continuous sector to keep the equation stable as the system works like a spline fitting process over potential values and e) radial distortion (James & Robson, 2014). Figure 25 shows the elevation error map generated in ArcGIS software between GNSS and DEM elevation datasets.



Resolution: 0.970211 m/pix
Point density: 1.06235 points per sq m

Figure 24: Elevation map of Imagery 1 Draganfly X4P Dataset

The Draganfly X4P is flown at different elevations over the selected survey site ranging from 15 metres to 45 metres above the ground surface to collect imagery datasets. Images collected by UAV's flown at a lower elevation from the ground produces greater resolution images but less image overlap and a UAV flown at higher elevation from the ground produces lower resolution images but greater image overlap.

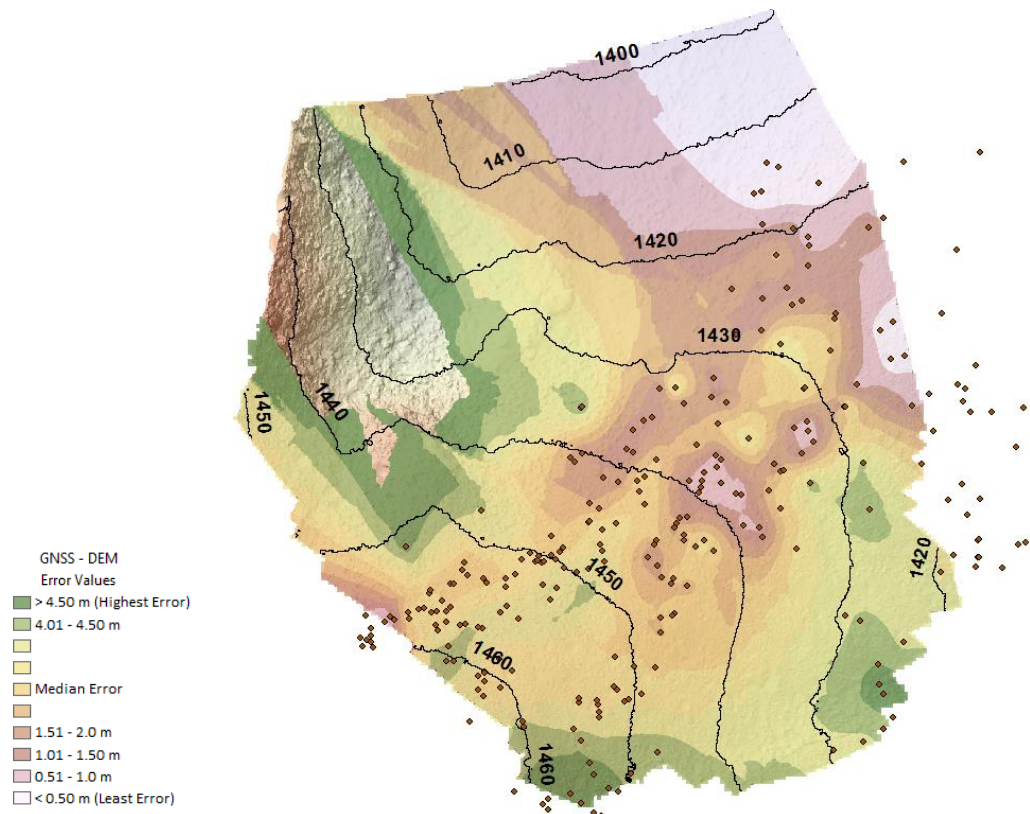


Figure 25: GNSS versus DEM elevation profile error map at Te Maari

The dots in Figure 25 represent the ground truthing data collected using Trimble R8 and TSC3 controller prior to the UAV imagery collection. Ground truthing and physical field analysis is a time-consuming process and usually results in the least amount of ground area able to be covered and recorded. The Draganfly X4P could cover a larger extent area surrounding the ground truthed survey site. The data on top left hand corner from Figure 25 was unable to be generated as there was no ground truth elevation survey data in that location. Due to this the elevation error margins were unable to be developed. The overall elevation errors can be drastically reduced by the inclusion of oblique images at various angles during image collection of the ground surface.

5.2 Conclusions from Data

Fitzgerald's (2014) orthophoto analysis produced a total of 3587 volcanic craters with crater diameters ranging between 0.3 m to 0.8 m, up to 2.3 km from the vents. A LiDAR was commissioned following the 6th August hydrothermal eruptions from the Upper Te Maari craters. This survey was conducted from a flight altitude of 1200 metres using the pre-event 10 m ASCII raster file DEM supplied by GNS Science. Fitzgerald mapped 107 craters from LiDAR imagery for the same survey area when compared to the 135 craters detected using Draganfly UAV and SfM workflow processes. In this project, SfM-derived orthophotos and 3D models from Draganfly X4P and Sony RX100, mimicked real life ground surface showing change in variation of ground surface. Twenty-eight additional volcanic craters were identified using SfM orthophotos when compared to LiDAR for the same region, even though it was mapped four years post 2012 Te Maari volcanic eruptions.

Location of 135 volcanic craters using a model builder at Te Maari

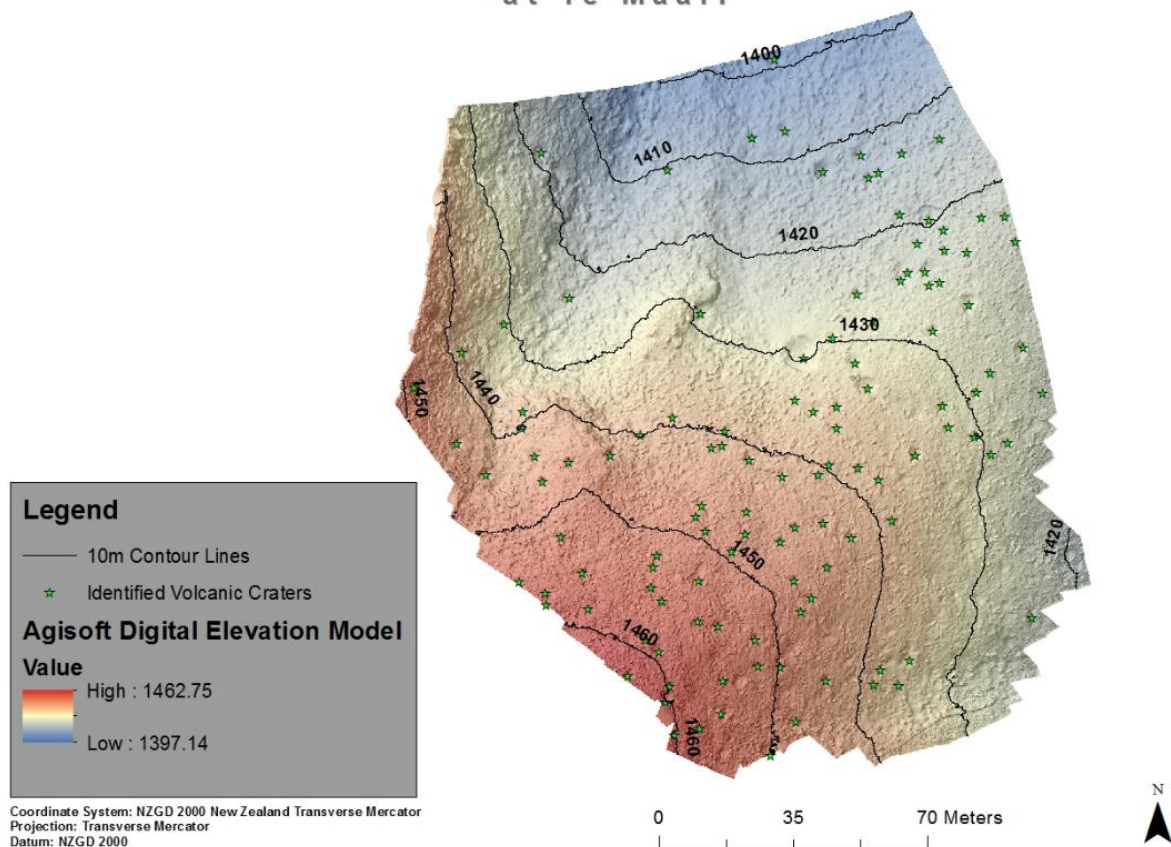


Figure 26: Locations of 135 volcanic craters identified using a model builder

Table 5 shows the different aerial and ground survey techniques available currently to compare heights, resolution, scale, time and costs involved for each technique. Handheld SfM photogrammetry, GNSS ground truthing and 3D scanning methods consume a greater amount of time to cover very little ground area on foot. The UAV's, LiDARs and other aerial methods are generally suited to cover a larger area in a short time span. The accuracies of UAV DEM's depends on various factors especially the ground control target positioning and equipment used to survey the region. Comparisons between UAV, LiDARs, GNSS survey methods, 3D scanning techniques and close range SfM photogrammetry shown in Table 5 provides information which help the user in planning future projects.

Table 5: Comparison of different techniques and survey styles

Technique for modelling	Close Range SfM (Ground Based, handheld)	UAV (Type 1 - 20m flight)	UAV (Type 2 - 40m flight)	GNSS Ground Truthing	2012 Tongariro LiDAR Survey (Procter et al., 2014)	Traditional LiDAR Surveys (Means et al., 2000) (Kolzenburg et al., 2016)	Traditional Laser Scanning (Baltsavias, 1999) (Rocchini, Cignoni, Montani, Pingi, & Scopigno, 2001)
Total area of site	20 m ²	100 to 120 m ²	100 to 120 m ²	100 to 120 m ²	Few km ²	Recommended for larger areas due to costs involved	Ideally used in the construction and building industry for civil engineering projects
Measurement distance (above ground)	1.5 to 2 m	20 m	40 m	Ground level	1200 m	~ 2000 m	Ground level
Equipment needed	Camera, monopod, auto-click feature	Multi-rotor UAV system, GPS camera, batteries	multi-rotor UAV system, GPS camera, batteries	High end R8, R10 models necessary to achieve greater accuracies.	Optech ALTM 3100EA LiDAR system, Trimble AIC medium format digital camera, RTK GPS	Airplanes, GPS base station (within 50km), LiDAR systems, laser scanners and sensors	Multi-station base, higher end survey equipment like total station equipment. Storage data of large files
Costs involved including	\$100 to \$1000	\$5000 to \$10000	\$5000 to \$10000	From \$5000	n/a	Minimum flight operation costs involved.	From \$15,000

equipment, labour (USD)						Up to \$30,000 \$300 to \$450 per mi ²	
Time consumed for data captured	60 to 90 min	flight time 45 mins	flight time 45 mins	10 hours	2 days 8 th and 9 th Nov 2012	Depends on area covered	1 day
Number of images/points captured	70 to 90 images	230 to 250 images	120 to 140 images	up to 300 to 350 point features	Thousands	Thousands of features (depends on area covered)	Depends on the project. Raw data compiles above 80 GB worth of data
Time taken for data processing/ data modelling	4 hours	10 hours	6 hours	4 hours	n/a	Approximately 4 to 6 weeks	2 weeks
Resolution	High	High	Med - High	n/a	High (2012 LiDAR 1m resolution hill shaded DEM LINZ Topographic map contour derived 10m resolution, hill shaded DEM)	High (50cm, 1m TIFF images possible in some cases)	n/a
Accuracy	Errors more pronounced	Med-High error. Depends on the	Med-High error. Depends on the	High (For higher accuracy ground	Manufacturer's specification 0.25 m horizontal accuracy	High	High (RMS error 2 mm horizontal and 3mm vertical)

		processes and equipment used	processes and equipment used	truthing projects, it is recommended to use total station survey equipment)	0.15 m open ground elevation accuracy		
--	--	------------------------------	------------------------------	---	---------------------------------------	--	--

Handheld mobile laser scanners (HMLS) provide a new ground based approach for mobile data collection of topographic data. It provides an alternative for ground based terrestrial laser scanners (TLS). The TLS survey times are significantly increased in complex topographic environments due to its tripod mount set up. The application of SfM and multi view stereo (MVS) three dimensional algorithms have enabled DEM generation by using a UAV mount laser scanner setup. HMLS style of survey is approximately forty times faster than TLS and six times faster than SfM-MVS style of surveying (James & Quinton, 2014).

5.2.1 Technical aspects, limitations and costs involved

LiDAR: LiDAR projects costs depend upon project specifications. A 1m point spacing project over moderate terrain would be more expensive than a 3m point spacing project. The price estimates also depend upon location, terrain type, vegetation and time of the year. A processing time of 4 to 6 weeks is further required to generate bare earth DEMs, reflective surface DEMs, intensity images, ground survey reports, point cloud data and LiDAR derived land cover reports. The pricing also varies on the accuracy of the survey. For surveys with a less accuracy tolerance, higher flight heights can be used allowing a wider swathe. Lower flight heights enable greater accuracy producing better quality surveys (Kolzenburg et al., 2016).

Acquiring LiDAR data involves high cost and many factors influence the acquisition process. A LiDAR survey is conducted from an aircraft by shooting an airborne laser on to the ground surface; and is reflected back to the sensor on the aircraft that measures the elapsed time between the laser shot and reflection (Tilley, Munn, Evans, Parker, & Roberts, 2004). High density mapping greatly increases the costs when compared to the traditional methods, such as field work and analysis. The overall results from a LiDAR survey could take 4-6 weeks to be generated costing greater than \$30,000 USD (Renslow, Greenfield, & Guay, 2000).

SfM: SfM has a huge cost advantage over LiDAR surveys. Although the higher end UAVs costs up to \$20k USD, reliable quadcopters, octocopters and drones are available from \$5k - 10k USD. The investment in UAVs is one-off and this set up can be used for multiple projects across various studies. Agisoft Photoscan Pro educational license and Sony RX100 camera system costs \$549 USD and \$900 USD respectively.

GNSS ground truthing equipment: Trimble's R8s and R10s are the more advanced versions of GPS data collection and the equipment costs from \$5000 USD. There are no operational costs involved to run an SfM model and a basic DEM can be developed within two days on an advanced computing platform. The open source free SfM software technology and budget UAV systems allow users to minimize the operational costs.

Laser Scanning: Laser scanners create point cloud data which requires 3D software such as FARO Scene 3D or Trimble Realworks software. Laser scanning is an evolving technology used in the construction industry. The major limitation is processing time of large files of data and costs (Means et al., 2000).

Large scale projects rely upon LiDAR and remote sensing methods. The application and uses of LiDAR are in many different fields such as agriculture, oil and gas exploration, mining, forestry planning and management, military, and tsunami models. The accuracy of the model not only depends on the aerial imagery and survey datasets but heavily dependent on atmospheric conditions and other technical aspects. Strong winds produce air turbulence for the drones causing blurred spots on images which need be manually removed using Photoshop software. Such tasks can be time consuming if majority of the aerial imagery datasets have blurred spots (Siebert & Teizer, 2014). To get the results that suit the projects requirement using UAV systems, it is important to understand the accuracy requirements of the project along with equipment needed to achieve that accuracy. SfM is to be preferred when imaging open sites that are not occluded by trees and buildings. It is easier to mobilize a small UAV easily for small mapping projects or emergency purposes. LiDAR should be preferred when modelling narrow sharp objects such as ground pipeline networks; and if the ground is obstructed by tree

canopy (Charlton, Large, & Fuller, 2003; Jones, Brewer, Johnstone, & Macklin, 2007).

5.3 Considerations for future SfM field methods

The combination of UAV and SfM technology is a useful tool for future researchers for mapping volcanic hazard deposits. It provides users with a unique visual perspective, allowing for better volcanic impact monitoring, modelling and management. Some of the photo acquisition considerations for future SfM fieldwork include:

- Take photos of the survey site at a single height and then either increase or decrease depending on the resolution requirement. The difference in elevation is used to create error maps using GIS software.
- The edges of the SfM model of survey site will have a lower photo density, so always photograph a larger area than the survey site. Resolution is important when considering the overlap of images. A lower resolution model does not require high overlap as it significantly increases processing time. It is critical that the area of interest is covered by at least 70% of image overlap.
- When the lighting is too dark, the texture of the ground does not stand out and if it is too bright, the features appear washed out. For small scale projects, take photographs when there is lower lighting with the sun still out.
- Natural geologic outcrops are not always clearly visible in the model so geo-reference more ground targets across the survey site instead. Avoid shiny surfaces when using ground control targets such as glass, mirror, metallic paint and adopt a numbered ground target model.

- If the UAV cannot cover the entire area in a single flight, break the area into smaller areas and note down the photo sequence in the field notebook. Reduce the resolution of the images and create the SfM model to reduce computer workload and processing time if overall accuracy is not critical.

5.4 Hazard Risks and Management of UAV hazards

Table 6: Hazard risk assessment and management when conducting UAV Sfm flight

Hazard Description	Significance (Yes/No)	Location of hazardous event	Control Plan	Eliminate (E), Isolate (I) or Minimize (M)
UAV batteries may combust spontaneously and this may cause the fragments to fly in random directions and catch fire with the dry grass during flight or while carrying	Yes	Proximity to the UAV and storage area	A small fire extinguisher to be accompanied to put out any fire that could be ignited. Batteries need to be placed in a Lithium-Polymer fireproof pouch to avoid any fire risk	I
Loss of control of UAV. Failure of auto pilot system due to strong wind gusts, power loss, rotor damage or bird strike	Yes	Proximity to the UAV	Fly UAV away from public. Spotter looks out for other hazards such as battery level, secondary air flights and birds while the pilot focusses on UAV	I
Rotor injury during UAV take-off and landing	Yes	Proximity to the UAV	Perform take-off and landing on a flat surface away from public	I

Tourism, commercial low flying airplanes in contact with UAV	Yes	Proximity to the UAV	Lower the UAV below 100 metres or perform immediate landing if the pilot/spotter spots a secondary aircraft within 2 km of survey site.	E
Heat stroke/Sun exhaustion	No	Too much exposure to the sun and dehydration	Plenty of water intake during fieldwork. Appropriate clothing such as sun screens, hat necessary.	E
Tripping hazards on uneven surface	Yes	Hilly and uneven terrain	Exercise caution when moving around, wear sturdy footwear and carry medical kits	M
Active volcanic environment – possibility of a volcanic eruption	Yes	Eruption of pyroclastic currents, ballistics, steam and ash	Limit time within active hazard zones. Check current activity from local organizations who monitor signs of activity	M

Chapter 6: Conclusion

Chapter 6 presents the conclusions of this thesis. It primarily draws from the research and results presented in Chapters 3 and 4, but also from the discussion presented in Chapter 5. Through the study of UAV and SfM technology and comparing its results against other survey methods, the following conclusions have been drawn:

- Like LiDAR surveys, UAV-SfM surveys also depend on low flight altitudes to achieve greater accuracy. UAV-SfM modelling accompanied with GNSS ground truthing survey methods allow for quick and cost effective generation of DEM's during emergencies.
- Processing and modelling the raw data from LiDAR and laser scanning surveys requires 3 – 6 weeks of time when compared SfM methods, which only requires one or two days to generate high to medium spatial resolution DEM's.
- The error margins observed between GNSS and SfM elevation datasets can be reduced for future projects by incorporating oblique imagery datasets in to SfM software. This enables better overlap of photographs, better linking of features and less overall distortion of the ground surface.
- The UAV-SfM method and workflow identified more craters than LiDAR surveys of a 100 m² area from the 2012 Te Maari eruptions. However, LiDAR surveys have a greater advantage especially when mapping a larger area when compared to UAV surveys.

- It is critical to understand the accuracy and resolution requirements of the project to decide which survey method suits best. Section 5.2 provides a detailed summary of the technical requirements and limitations attached to each survey style.

The UAV aerial mapping and SfM generated DEM analysis revealed 135 volcanic impact craters within a 100 m² area from 2012 Te Maari eruptions at a resolution of 118ppcm, when compared to 107 volcanic craters identified through Te Maari LiDAR survey. UAV-SfM methods are capable to generate hazard models and distribution maps at high spatial resolutions during emergency scenarios, therefore it remains a powerful tool which can be used for mapping purposes in the field of volcanology. This thesis found that the combination of UAV and SfM technology associated workflow can be used very effectively to cover small projects and particularly following emergencies. These cost-effective methods can therefore be used at localised sites to achieve maximised results with moderate errors, when compared to laser scanning LiDAR survey methods. However, for large scale high resolution and accuracy projects, LiDAR is preferred due to its ability of converting the precise laser pulse measurements over a swathe of terrain, into accurate ground elevation using a GPS to develop digital elevation models.

References

Advanced Geodetic Surveys (2016). Used Trimble R8 GNSS Model 4 System.

Retrieved from <https://www.agsgps.com/product/used-trimble-r8-gnss-model-4-system/>.

Agisoft (2017). System Requirements Recommended Hardware.

Retrieved from <http://www.agisoft.com/downloads/system-requirements/>

Bakula, M. (2013). Study of reliable rapid and ultrarapid static GNSS surveying for determination of the coordinates of control points in obstructed conditions. *Journal of Surveying Engineering*, 139(4), 188-193.

Baltsavias, E. P. (1999). A comparison between photogrammetry and laser scanning. *ISPRS Journal of photogrammetry and Remote Sensing*, 54(2), 83-94.

Breard, E., Lube, G., Cronin, S., Fitzgerald, R., Kennedy, B., Scheu, B., . . . Procter, J. (2014). Using the spatial distribution and lithology of ballistic blocks to interpret eruption sequence and dynamics: August 6 2012 Upper Te Maari eruption, New Zealand. *Journal of Volcanology and Geothermal Research*, 286, 373-386.

Charlton, M. E., Large, A. R., & Fuller, I. C. (2003). Application of airborne LiDAR in river environments: the River Coquet, Northumberland, UK. *Earth surface processes and landforms*, 28(3), 299-306.

Crouch, J. F., Pardo, N., & Miller, C. A. (2014). Dual polarisation C-band weather radar imagery of the 6 August 2012 Te Maari eruption, Mount Tongariro, New Zealand. *Journal of Volcanology and Geothermal Research*, 286, 415-436.

- Department of Conservation (2017). Volcano Risk in Tongariro National Park.
Retrieved from <http://www.doc.govt.nz/parks-and-recreation/places-to-go/central-north-island/places/tongariro-national-park/know-before-you-go/volcanic-risk-in-tongariro-national-park/>.
- Draganfly (2017). Draganflyer X4-P.
Retrieved from <http://www.draganfly.com/products/x4-p/specs>.
- Eisenbeiss, H., & Zhang, L. (2006). Comparison of DSMs generated from mini UAV imagery and terrestrial laser scanner in a cultural heritage application. *International Archives of Photogrammetry, Remote Sensing and Spatial Information Sciences*, 36(5), 90-96.
- Fitzgerald, R. H. (2014). An assessment of ballistic hazard and risk from Upper Te Maari, Tongariro, New Zealand.
- Hobden, B. (1997). Modelling magmatic trends in time and space: eruptive and magmatic history of Tongariro volcanic complex, New Zealand.
- James, M. R., & Quinton, J. N. (2014). Ultra-rapid topographic surveying for complex environments: the hand-held mobile laser scanner (HMLS). *Earth surface processes and landforms*, 39(1), 138-142.
- James, M. R., & Robson, S. (2014). Mitigating systematic error in topographic models derived from UAV and ground-based image networks. *Earth surface processes and landforms*, 39(10), 1413-1420.
- Javernick, L., Brasington, J., & Caruso, B. (2014). Modeling the topography of shallow braided rivers using Structure-from-Motion photogrammetry. *Geomorphology*, 213, 166-182.
- Jolly, A., Jousset, P., Lyons, J., Carniel, R., Fournier, N., Fry, B., & Miller, C. (2014). Seismo-acoustic evidence for an avalanche driven phreatic eruption through a

- beheaded hydrothermal system: an example from the 2012 Tongariro eruption. *Journal of Volcanology and Geothermal Research*, 286, 331-347.
- Jones, A. F., Brewer, P. A., Johnstone, E., & Macklin, M. G. (2007). High-resolution interpretative geomorphological mapping of river valley environments using airborne LiDAR data. *Earth surface processes and landforms*, 32(10), 1574-1592.
- Kolzenburg, S., Favalli, M., Fornaciai, A., Isola, I., Harris, A., Nannipieri, L., & Giordano, D. (2016). Rapid Updating and Improvement of Airborne LIDAR DEMs Through Ground-Based SfM 3-D Modeling of Volcanic Features. *IEEE Transactions on Geoscience and Remote Sensing*, 54(11), 6687-6699.
- Langley, R. B. (1999). Dilution of precision. *GPS world*, 10(5), 52-59.
- Lube, G., Breard, E. C., Cronin, S. J., Procter, J. N., Brenna, M., Moebis, A., . . . Fournier, N. (2014). Dynamics of surges generated by hydrothermal blasts during the 6 August 2012 Te Maari eruption, Mt. Tongariro, New Zealand. *Journal of Volcanology and Geothermal Research*, 286, 348-366.
- Lucieer, A., Robinson, S., Turner, D., Harwin, S., & Kelcey, J. (2012). Using a micro-UAV for ultra-high resolution multi-sensor observations of Antarctic moss beds.
- Maguire, C. (2014). Using Unmanned Aerial Vehicles and " Structure from Motion" Software to Monitor Coastal Erosion in Southeast Florida.
- Mancini, F., Dubbini, M., Gattelli, M., Stecchi, F., Fabbri, S., & Gabbianelli, G. (2013). Using unmanned aerial vehicles (UAV) for high-resolution reconstruction of topography: the structure from motion approach on coastal environments. *Remote Sensing*, 5(12), 6880-6898.

- Martin, L. (1980). An assessment of soil roughness parameters using stereophotography. *Assessment of Erosion*, 237-248.
- McGlone, C., Mikhail, E., & Bethel, J. (1980). Manual of photogrammetry.
- McGuire, M., Rys, M., & Rys, A. A Study of How Unmanned Aircraft Systems Can Support the Kansas Department of Transportation's Efforts to Improve Efficiency, Safety, and Cost Reduction.
- Means, J. E., Acker, S. A., Fitt, B. J., Renslow, M., Emerson, L., & Hendrix, C. J. (2000). Predicting forest stand characteristics with airborne scanning lidar. *Photogrammetric Engineering and Remote Sensing*, 66(11), 1367-1372.
- Miller, J., Morgenroth, J., & Gomez, C. (2015). 3D modelling of individual trees using a handheld camera: Accuracy of height, diameter and volume estimates. *Urban Forestry & Urban Greening*, 14(4), 932-940.
- Navidi, W. C. (2006). *Statistics for engineers and scientists* (Vol. 1): McGraw-Hill New York.
- Niethammer, U., Rothmund, S., James, M., Travelletti, J., & Joswig, M. (2010). UAV-based remote sensing of landslides. *International Archives of Photogrammetry, Remote Sensing and Spatial Information Sciences*, 38(Part 5), 496-501.
- Pardo, N., Cronin, S. J., Németh, K., Brenna, M., Schipper, C. I., Breard, E., . . . Agustín-Flores, J. (2014). Perils in distinguishing phreatic from phreatomagmatic ash; insights into the eruption mechanisms of the 6 August 2012 Mt. Tongariro eruption, New Zealand. *Journal of Volcanology and Geothermal Research*, 286, 397-414.

- Peter Heng, B., Chandler, J. H., & Armstrong, A. (2010). Applying close range digital photogrammetry in soil erosion studies. *The Photogrammetric Record*, 25(131), 240-265.
- Pollefeys, M., Van Gool, L., Vergauwen, M., Verbiest, F., Cornelis, K., Tops, J., & Koch, R. (2004). Visual modeling with a hand-held camera. *International Journal of Computer Vision*, 59(3), 207-232.
- Prakash, N. U., Vasantharaj, R., Balasubramanian, E., Bhushan, G., Das, S., & Eqbal, F. (2014). Design, Development and Analysis of Air Mycoflora Using Fixed Wing Unmanned Aerial Vehicle (UAV). *淡江理工學刊*, 17(1), 1-8.
- Procter, J., Cronin, S., Zernack, A., Lube, G., Stewart, R., Nemeth, K., & Keys, H. (2014). Debris flow evolution and activation of an explosive hydrothermal system. *Te Maari, Tongariro, New Zealand (in this issue)*.
- Renslow, M., Greenfield, P., & Guay, T. (2000). Evaluation of multi-return LIDAR for forestry applications. *US Department of Agriculture Forest Service-Engineering, Remote Sensing Applications*. <http://www.ndep.gov/USDAFS/LIDAR.pdf> [Consulta: 12 de marzo de 2009].
- Robock, A. (2000). Volcanic eruptions and climate. *Reviews of Geophysics*, 38(2), 191-219.
- Rocchini, C., Cignoni, P., Montani, C., Pingi, P., & Scopigno, R. (2001). *A low cost 3 D scanner based on structured light*. Paper presented at the Computer Graphics Forum.
- Siebert, S., & Teizer, J. (2014). Mobile 3D mapping for surveying earthwork projects using an Unmanned Aerial Vehicle (UAV) system. *Automation in Construction*, 41, 1-14.

- Tilley, B. K., Munn, I. A., Evans, D. L., Parker, R. C., & Roberts, S. D. (2004). Cost considerations of using LiDAR for timber inventory. *Southern Forest Economics Workers. Online papers.*
- Turner, D., Lucieer, A., & Watson, C. (2012). An automated technique for generating georectified mosaics from ultra-high resolution unmanned aerial vehicle (UAV) imagery, based on structure from motion (SfM) point clouds. *Remote Sensing*, 4(5), 1392-1410.
- Viera, A. J., & Garrett, J. M. (2005). Understanding interobserver agreement: the kappa statistic. *Fam Med*, 37(5), 360-363.
- Westoby, M., Brasington, J., Glasser, N., Hambrey, M., & Reynolds, J. (2012). 'Structure-from-Motion' photogrammetry: A low-cost, effective tool for geoscience applications. *Geomorphology*, 179, 300-314.